The importance of lithofacies control on fluid migration in heterogeneous aeolian formations for geological CO2 storage: Lessons from observational evidence and modelling of bleached palaeoreservoirs at Salt Wash Graben, Utah

Newell, A, Pourmalek, A, Shariatipour, SM & Butcher, AS

Author post-print (accepted) deposited by Coventry University's Repository

Original citation & hyperlink:
Newell, A, Pourmalek, A, Shariatipour, SM & Butcher, AS 2019, 'The importance of lithofacies control on fluid migration in heterogeneous aeolian formations for geological CO2 storage: Lessons from observational evidence and modelling of bleached palaeoreservoirs at Salt Wash Graben, Utah', International Journal of Greenhouse Gas Control, vol. 91, 102841.
https://dx.doi.org/10.1016/j.ijggc.2019.102841

DOI 10.1016/j.ijggc.2019.102841
ISSN 1750-5836

Publisher: Elsevier

NOTICE: this is the author's version of a work that was accepted for publication in *International Journal of Greenhouse Gas Control.* Changes resulting from the publishing process, such as peer review, editing, corrections, structural formatting, and other quality control mechanisms may not be reflected in this document. Changes may have been made to this work since it was submitted for publication. A definitive version was subsequently published in International Journal of Greenhouse Gas Control, 91,(2019) DOI: 10.1016/j.ijggc.2019.102841

© 2019, Elsevier. Licensed under the Creative Commons Attribution-NonCommercial-NoDerivatives 4.0 International
http://creativecommons.org/licenses/by-nc-nd/4.0/10.1016/j.ijggc.2019.102841

Copyright © and Moral Rights are retained by the author(s) and/ or other copyright owners. A copy can be downloaded for personal non-commercial research or study, without prior permission or charge. This item cannot be reproduced or quoted extensively from without first obtaining permission in writing from the copyright holder(s). The content must not be changed in any way or sold commercially in any format or medium without the formal permission of the copyright holders.

The importance of lithofacies control on CO_2-charged fluid migration in heterogeneous aeolian formations: lessons from observational evidence and modelling of bleached palaeoreservoirs at Salt Wash Graben, Utah

Andrew J Newell*[a], Azadeh Pourmalek[b], Andrew S Butcher[a], Seyed Shariatipour[b] [a]British Geological Survey, Maclean Building, Wallingford, OX10 8BB [b]Faculty of Engineering, Environment and Computing, Fluid and Complex Systems Research Centre,

Coventry University, Coventry CV1 2NL, UK

*ajn@bgs.ac.uk

Abstract

Exhumed bleached palaeoreservoirs provide a means of understanding fluid flow processes in geological media because the former movement of fluids is preserved as visible geochemical changes (grey bleaching of continental red-beds). The bleached palaeoreservoirs of the Jurassic Entrada Sandstone occur in a region (Utah) where there are high fluxes of naturally-occurring CO2 and form outcrop analogues for processes related to geological storage of CO2. In this paper a bleached palaeoreservoir now exposed at outcrop is used to test the importance of geological heterogeneity on fluid flow. The bleached palaeoreservoir is developed in 'wet aeolian' lithofacies composed of alternating layers of sandstone and cemented muddy sandstone that range across three or more orders of magnitude in permeability. Despite these permeability contrasts the bleaching shows a remarkably uniform distribution within the palaeoreservoir that crosses lithofacies boundaries. Evidence from bleaching therefore suggests that geological heterogeneity within the range 1-10^3 millidarcies should not greatly impede the relatively uniform distribution of low-viscosity CO_2 charged fluids throughout a reservoir: a conclusion that has been substantiated here by flow modelling. Residence time is an important factor and where flows are transient the distribution of bleaching and modelling shows that flows are confined to high-permeability lithofacies.

Keywords

CO_2 storage, bleached palaeoreservoir, aeolian, Entrada Sandstone

1 Introduction

To stabilize atmospheric CO_2 and limit the impacts of global warming, considerable and constant reduction of greenhouse gas emissions is required (Ennis-King and Paterson, 2005). Carbon capture and storage (CCS) is an option that can be applied to stabilize CO_2 concentrations in the atmosphere at a level of 550 ppmv (IPCC, 2005). In this three-step technology, CO_2 is captured from large point sources such as fossil-fuel power plants, transported to the storage site where it is stored in the geological media for at least 10,000 years (Bickle and Kampman, 2013) and storage losses should not exceed 0.1 % per year (Pruess, 2006). Geological media considered for CO_2 geological storage are depleted oil and gas reservoirs, deep saline aquifers, unminable coal beds and potentially basalts (Bachu, 2008). Among these media only depleted oil and gas reservoirs (e.g. The CO_2CRC Otway Project) and deep saline aquifers (e.g. Sleipner Project) have been effectively established at pilot and commercial scales.

The behaviour of CO_2 in the subsurface significantly depends on its physical properties. For temperature and pressures above the critical point (31.18 °C and 73.9 bar), CO_2 is in a supercritical state. Supercritical CO2 has liquid-like density and gas-like viscosity that occupies the entire accessible volume of the reservoir (Bachu, 2000). A combination of physical (i.e. structural and stratigraphic trapping mechanism and residual or capillary trapping mechanism) and chemical trapping mechanisms (i.e. dissolution and mineral trapping mechanism) are involved in the CO_2 storage process. The optimum storage depth is around 800-1000 m since there is no significant benefit to store CO_2 at greater depths (Ennis-King and Paterson, 2002). The CO_2 density at this depth is still less than the density of the formation brine. Therefore, injected CO_2 migrates upwards under buoyancy and accumulates in structural traps which refer to a geological media with high-permeability overlain and surrounded by low-permeability topseal with high capillary entry pressure, whose shape inhibits the upward and lateral migration of the buoyant fluid (IPCC, 2005; Bachu, 2008; Lu et al., 2013). Structural traps can be classified into fold-dominated (e.g. In Salah CO_2 storage project) and fault-dominated (e.g. The CO_2CRC Otway Project) traps. Consequently, structural traps are geometries in which buoyancy-driven migration of CO_2 is restricted by folded or faulted rocks. Fold-dominated traps are by far the most important type of traps and purely fault-dominated traps are relatively rare (Biddle and Wielchowsky, 1994). Additionally, faults can be preferential flow path and also permeability barriers (Salvi et al., 2000).

There are significant uncertainties in modelling the fate of the injected CO_2 over a long time period (Pourmalek and Shariatipour, 2019). Natural CO_2 fields, as analogues for CO_2 storage projects, may provide new insight regarding CO_2 long-term fate (dissolution in the brine, reaction with rock minerals, escape via faults, and corroding topseals) in the subsurface (Bickle and Kampman, 2013). In some places CO_2 is actively escaping from natural reservoirs (e.g. Little Grand Wash and Salt Wash Graben in central Utah, USA), primarily along faults, but elsewhere CO_2 has been securely stored in geological formations for geological periods of time (e.g. Bravo Dome and McElmo CO_2 fields, Colorado Plateau and Southern Rocky Mountains region, USA) and have been produced for commercial purposes (Allis et al., 2001).

The study of potential subsurface reservoirs and aquifers for CO_2 storage is challenging and expensive by nature and gaining knowledge on possible geological controls on fluid movement is mainly obtained by seismic survey and well data such as core and downhole geophysical logs. Such subsurface data sets tend to leave a knowledge gap between the relatively coarse scale of seismic interpretation and the fine scale of information from wells. In the hydrocarbons industry, the study of rock outcrop has long been used as a means of filling this knowledge gap, providing analogue information on the shape and dimensions of geological heterogeneities at the metre to decametre scale. In recent years new technologies such as terrestrial laser scanning has greatly increased the range of information derived from outcrop studies (Howell et al., 2014), however, a disadvantage of most analogue information remains, that is, the difficulty of making any direct link between the observed geological heterogeneity at outcrop and the likely impact on fluid movement in the subsurface. It is here that the study of outcrops that represent palaeoreservoir systems becomes important, and more specifically, those palaeoreservoirs where the former presence and migration of fluids has left a permanent fingerprint through chemical alteration of the rock matrix. A common example of this fingerprint is the grey bleaching of red-bed terrestrial sandstones by reducing fluids. This phenomenon is particularly widespread across the Colorado Plateau of the southwestern United States where the bleaching of reddened Mesozoic sandstones by reducing fluids such as methane, carbon dioxide and hydrogen sulphide provides a visually striking record of their pathway through permeable sandstones and fractures (Beitler et al., 2003; Chan et al., 2000; Haszeldine et al., 2005; Wigley et al., 2012).

The significance of bleached palaeoreservoirs for understanding fluid flow in the subsurface has long been realized (Beitler et al., 2003; Chan et al., 2000), but in recent years has seen a resurgence of research activity because of the realisation that bleaching caused by large fluxes of CO_2-charged fluids on the Colorado Plateau provides an opportunity to improve our understanding of the processes associated with geological carbon storage as part of climate change mitigation strategies (Bickle and Kampman, 2013; Bickle et al., 2013; Burnside et al., 2013; Wigley et al., 2013). Much of this recent outcrop analogue work has focussed on bleached palaeoreservoirs hosted within Jurassic red-bed formations of eastern Utah and has had a strong emphasis on the role of fractures in fluid flow (Dockrill and Shipton, 2010), the geochemistry of rock-fluid interaction (Bickle et al., 2013; Kampman et al., 2016) and the longterm integrity of CO_2-reservoir topseals (Kampman et al., 2016).

This paper describes a new application of the bleached Jurassic palaeoreservoirs of the Colorado Plateau that explores the relationship between the distribution of bleaching caused by the movement of CO_2-charged fluids and the primary depositional fabric of the reservoir rocks. In doing so we seek to address three main questions. (1) What does the bleached palaeoreservoir tell us about the importance of lithofacies control on the movement of CO_2charged fluids, particularly at geological time-scales? (2) Can flow simulators, which are critical to understand the feasibility and long-term security of geological carbon storage, successfully replicate the distribution of bleaching observed in the reservoir analogue and clarify potential pathways? (3) Does the palaeoreservoir provide insight into how much geological heterogeneity and complexity needs to be incorporated into static geological models (increasing the time and cost of computer simulation) for the realistic modelling of CO_2 sequestration? While many authors have studied the bleached palaeoreservoirs around Green River in connection with CO_2 storage (Bickle et al., 2013; Kampman et al., 2016 and Dockrill and Shipton, 2010) there has been no attempt to construct a reservoir scale flow model to try and replicate the observed patterns of bleaching (an outcrop proxy for the distribution of CO_2-charged reducing-fluids) and investigate the regional pathways for the ingress of buoyant CO_2-charged fluids into the former reservoir.

The rocks under discussion are part of the Middle Jurassic Entrada Sandstone exposed near Green River in Utah, which have been the subject of much recent CO_2 storage-related research (Kampman et al., 2014; Kampman et al., 2016). The Entrada Sandstone is considered a classic example of what sedimentologists refer to as a 'wet aeolian deposystem'. The term 'wet' denotes an aeolian deposition environment where the accretion of wind-blown sediment is regulated by a shallow water table (Bristow and Mountney, 2013; Crabaugh and Kocurek, 1993). Wet aeolian systems are distinguished from their more familiar 'dry aeolian' counterparts by the development of a highly layered sedimentary architecture with alternating beds of relatively high-permeability aeolian dune sandstone and low-permeability muddy interdune lithofacies. The Entrada Sandstone is potentially a good analogue for many Permian and Triassic red-bed aeolian-dominated reservoirs that are considered important targets for geological storage of CO_2 on the NW European continental shelf (Newell and Shariatipour, 2016).

2 Geological description of studied area

2.1 Location

The study site is located 13 km south of the town of Green River in east central Utah (38.865N 110.098W) on a WNW-ESE trending fault system, which in most recent published literature is called the Salt Wash Graben (Ogata et al., 2014; Pearce et al., 2011; Wigley et al., 2013) (Figure 1).

2.2 Entrada Sandstone

The focus of this study is the Middle Jurassic Entrada Sandstone which at Salt Wash Graben ranges from 43 to 170 m thick and is subdivided into two members, the Slick Rock Member and the Earthy Member (Doelling, 2001) (Figure 2). The Slick Rock Member is typically an alternation of aeolian cross-bedded sandstone and wavy-laminated silty sandstone that interbed on a metre to decametre scale (Figure 3). The Slick Rock Member is significant for this study in forming the permeable palaeoreservoir rock for CO_2 charged fluids. The Earthy Member sharply overlies the Slick Rock Member and is a muddy fine-grained sandstone typically around 20-30 m thick. The Earthy Member forms the topseal on the aeolian sandstone reservoir. The Entrada Sandstone is considered a classic example of a 'wet aeolian dune system' where deposition was influenced by a shallow water table (Crabaugh and Kocurek, 1993).

2.3 Structure

The Entrada Sandstone under investigation forms an inlier on the crest of the Green River Anticline, an open, NNW plunging structure (Figure 1) that is one of a number of similarly trending salt-cored anticlines in the Paradox Basin (Pederson et al., 2013). The axis of the Green River Anticline is cut at a high angle by faults of the Salt Wash Graben and the Little Grand Wash Fault further to the north (Figure 1). The described Entrada Sandstone has a narrow elongate crop on the northern footwall block of the Salt Wash Graben (Figure 1). To the north of the Entrada Sandstone, an arcuate series of stepped scarps are formed by younger Jurassic and Cretaceous strata. To the south, the Entrada Sandstone is sharply truncated by the northern bounding fault of the Salt Wash Graben (Figure 4). The central part of this graben exposes Cretaceous Cedar Mountain Formation, indicating a downthrow of around 200 m. Immediately south of the fault, the Cretaceous strata within the graben dip at high angles (10-15 degrees) to the south. A number of faults also occur parallel to the Green River Anticline and form a north-south linkage between the Salt Wash Graben and Little Grand Wash Fault (Figure 1). Faults developed parallel to fold axes are a common feature of the Paradox Basin and may have developed in response to salt dissolution at shallow levels (Baars and Doelling, 1987), local stretching across the tops of drape anticlines, or the thinning of salt walls during regional extension (Ge and Jackson, 1998). The significance of the structure is that the Salt Wash Graben palaeoreservoir is located on the crest of the north-plunging Green River Anticline with an updip seal formed by downfaulted mudstone-rich Cedar Mountain Formation in the Salt Wash Graben. The reservoir was later breached by extensional fracturing along the fold crest.

2.4 Burial history

Reconstructions of the burial history of the Green River sector of the Paradox Basin show that here the Middle Triassic Entrada Sandstone at Salt Wash Graben was probably buried to depths approaching 2.5 km, before being rapidly exhumed and brought back to the surface from around the Oligocene onwards (Nuccio and Condon, 1996).

3 Field methods

The main objective of this study was testing the relationship between the distribution of bleaching and lithofacies-scale heterogeneity in the Entrada Sandstone. To achieve this, structural and stratigraphic mapping of the Entrada Sandstone was undertaken in a major area of grey bleaching that covers approximately 1.2 km^2 to the north of the Salt Wash Graben and is located on the crest of the Green River Anticline (Figure 1). Additional work was undertaken on a smaller area of bleached Entrada Sandstone 5 km to the southeast on the eastern flank of the anticline (Figure 1). Base maps were obtained from internet sources and included high resolution aerial photography, digital terrain models and geological maps (AGRC, 2018). Data were collected on geological boundaries, dip and strike of bedding, lithofacies, locations of major faults and fractures and the extent of bleaching throughout the palaeoreservoir. Sedimentary logs were measured in the Entrada Sandstone at the western and eastern end of the bleached zone (Figure 1). On each logged section, grain-size and sorting were determined from images taken with a laptop-attached digital microscope. Field measurements of sandstone permeability were taken using a TinyPerm II Portable Air Permeameter manufactured by New England Research (NER). This unit employs a mass flow meter to determine a pressure decay curve calibrated to permeability and is extremely portable and thus well-suited to outcrop measurements. Laboratory analysis on a representative set of field-collected samples has included the measurement of gas permeability in a pressurised core holder using nitrogen under steady state conditions and the determination of pore throat size distributions by mercury injection capillary pressure (MICP) tests. Samples were examined in thin section and under the scanning electron microscope to provide additional information on grain morphology, composition, pore-filling cements and clays. Full details of the petrography of the Entrada Sandstone at Salt Wash Graben are provided by Rushton et al. (2018).

4 Lithofacies of the Entrada Sandstone

4.1 Slick Rock Member – palaeoreservoir lithofacies

The Slick Rock Member is composed of a number of different sandstone-dominated lithofacies whose key characteristics are summarised in Table 1. The spectrum of the most common sandstone lithofacies is illustrated in Figure 6 which shows how the grain-size and sorting grades from clean (mud-free) sandstones, through silty sandstones, to sandstones that can contain a significant proportion of mud. This is usually accompanied a change in the predominant sedimentary structure from cross-bedding, to horizontal lamination, to wavy lamination and convolute bedding.

Aeolian dune sandstones are usually composed of clean, cross-bedded sandstone (Figure 6A). The sandstones are dominated by quartz with lesser amounts of K-feldspar and mica. Quartz grains typically range up to 0.4 mm in size and are rounded to subrounded with a frosted appearance (Figure 7). The sandstones have variable amounts of dolomite and calcite porefilling cement, which is often concentrated at bed tops, where clean sandstones are overlain by muddier sandstones. Elsewhere the sandstones have an open pore structure and high permeability. Laboratory measured gas permeability values are typically around 1600 mD in plugs cut parallel to lamination and 830 mD in plugs cut perpendicular to lamination. Porosity determined from MICP was usually around 25% which was connected by pore throats with a median diameter of 26.5 µm. The aeolian dune sandstones typically occur in beds up to 1 m thick and are commonly developed as a single set of cross-bedding composed of foresets that may have an angular relationship with the underlying bed, or merge tangentially into relatively flat-lying wind-ripple deposits (Figure 3). The presence of cross-bedding indicates that these sandstones were deposited on slip-faced dunes, probably on dry substrates elevated above the groundwater table where wind could generate bedforms from loose sand.

Wind-ripple laminated sandstones are compositionally similar to aeolian dune sandstones but are distinguished by a horizontal or low-angle lamination where fine-grained sand is concentrated into distinctive pin-stripe laminae (Figure 6B) by the migration of low amplitude wind ripples. These would have formed on dry mobile substrates around the flanks of dunes or on low relief aeolian sand sheets where dunes were absent.

Beds of clean aeolian dune and wind-rippled sandstone interbed with intervals of silty sandstone or clayey silty sandstone showing irregular wavy (Figure 6C) or highly convolute lamination (Figure 6D). These sandstones are fine-grained and well-cemented with dolomite and calcite, sharing many of the petrographic and reservoir properties (described below) of the overlying Earthy Member of the Entrada Sandstone. It is likely that these muddy sandstones with irregular lamination were deposited on damp or wet substrates within lowlying interdune areas that intersected the water table (Crabaugh and Kocurek, 1993). Windblown sand, silt and clay may have been deposited within these areas by adhering to the damp surface (Kocurek and Fielder, 1982). Salt crusts precipitated from saline groundwater may also have been important in trapping irregular patches of wind-blown sediment. The subsequent dissolution of salt may account for some of the highly convolute lamination, although the development of overpressure in groundwater confined by thin clay laminae may also have been important.

As established by previous work on the Entrada Sandstone, the sandstones of the Slick Rock Member were mostly, but not exclusively, deposited in a range of aeolian environments that interacted with a shallow groundwater table (Crabaugh and Kocurek, 1993; Kocurek, 1981). Wet and dry aeolian lithofacies within the Slick Rock Member of the Entrada Sandstone typically alternate on a scale of around one metre (Figure 5). Often the lithofacies are arranged in ‘drying-upward cycles’ where muddy wet interdune deposits pass upwards, through wavy laminated sandstones and wind-ripple laminated sandstones, into crossbedded aeolian dune sandstones. The aeolian dune sandstones have a high lateral continuity and can be mapped and correlated across the full extent of the palaeoreservoir. Crabaugh and Kocurek (1993) show how conditions of steady subsidence (or rising groundwater level) can produce a highly layered architecture in wet aeolian deposits whose geometry depends on the size of the dunes and the adjoining damp or wet interdune depressions, and the ratio between the lateral rate of bedform migration and the vertical trajectory of accumulation driven by relative water table rise (Bristow and Mountney, 2013).

4.2 Earthy Member – the topseal

The Earthy Member has the general appearance of a massive unit of well-cemented, reddish brown (where unbleached), silty sandstone sharply overlying the Slick Rock Member (see Figure 3). The mineralogy of the detrital grains is dominated by quartz grains with K feldspar and albite in less abundance. Grains are mostly in the coarse silt to very fine sand size and vary from subrounded to angular (Figure 7D). Calcite and dolomite are the major cementing phases and fill much of the intergranular space. These appear to predate extensive sediment compaction and thus probably formed as early diagenetic calcretes and dolocretes. Illitic clay minerals form a thin coating around many grains and occur as thin laminae and reworked clasts throughout the sandstone. Kaolinite is common as a grain-replacive diagenetic phase (Rushton et al., 2018). Typical laboratory determined permeability values are 0.38mD in the horizontal direction and 0.25mD in the vertical direction. The Earthy lithofacies had a MICP determined porosity of around 8% and a median pore throat diameter of 0.4 µm.

The Earthy Member has a highly variably sedimentary fabric. In some cases it consists of irregular pods and lenses of fine-grained sandstone separated by discontinuous and highly convolute beds of laminated silt and clay (Figure 6D). Individual sand pods have highly variable shapes and sizes but are usually less than 10 cm across and composed of fine-grained sand. Relatively clean sandstones also occur as thin (<0.5 m) discontinuous sheets of massive or flat laminated aeolian sandstone that are encapsulated within the more typical Earthy lithofacies and these probably represent small, localised, and discontinuous mounds of windblown sand. Some of the sandstones show small-scale cross-lamination which, in association with minor erosion surfaces overlain by reworked mudstone flakes, suggests a fluvial origin.

The Earthy Member is generally interpreted as the product of a sabkha or muddy sandflat environment in an arid marginal marine setting adjacent to the Utah-Idaho Trough (Kocurek, 1981). Sand, silt and clay was probably transported and deposited across the flat by a combination of marine inundation, fluvial sheet floods and aeolian processes, but the mostly high water table inhibited the formation of large aeolian bedforms. The formation of salt crusts and their subsequent dissolution may have contributed toward the trapping of windblown silt and sand and the formation of an irregular bedding fabric (Goodall et al., 2000).

5 Bleaching within the palaeoreservoir

5.1 Bleaching agent

A link between the bleaching of red-bed deposits and the migration of reducing fluids has long been established on the Colorado Plateau (Beitler et al., 2003; Chan et al., 2000; Haszeldine et al., 2005; Wright et al., 1962). Bleaching of red beds occurs whenever acidic or reducing fluids remove oxidised iron, usually present in terrestrial deposits as fine-grained haematite

(Fe_2O_3); a common early diagenetic grain coating developed in sediments deposited under humid but well-drained conditions (Sheldon, 2005; Walker et al., 1978).

Ferric (Fe^{3+}) iron is relatively insoluble but reduction to the more soluble ferrous (Fe^{2+}) iron allows its removal and sandstone decolouration. There are a range of possible reducing agents in sedimentary basins that include hydrocarbons, hydrogen sulphide (H_2S) and carbon dioxide (CO_2) (Schumacher, 1996), all of which occur in large accumulations across the Colorado Plateau (Craddock et al., 2017).

The composition of the reducing fluids that caused bleaching of the Entrada Sandstone at Salt wash Graben has the subject of much recent research with current consensus on CO_2-rich brines containing quantities of dissolved CH_4 (Bickle et al., 2013; Wigley et al., 2013; Wigley et al., 2012). Evidence for the migration and surface leakage of CO_2 is very well documented around Salt Wash Graben, where surface emissions occur as cool, saline-water springs preferentially located along faults and fractures, where they are associated with the build-up of tufa mounds (e.g. see Figure 4) dating back to at least 400,000 years (Burnside et al., 2013; Han et al., 2013; Kampman et al., 2012; Kampman et al., 2013; Pearce et al., 2011). The presence of pyrite pseudomorphs in the Entrada Sandstone at Salt Wash Graben may indicate the additional importance of H_2S as a bleaching agent (Rushton et al., 2018).

5.2 Regional fluid pathways

In the Paradox Basin, the reducing fluids are generally thought to have originated at depth and to have moved upwards through the permeability created by faults and then laterally into transmissive sandstone formations (Chan et al., 2000; Wigley et al., 2013). Given the present structural configuration of the Entrada Sandstone at Salt Wash Graben, the fluids could have migrated upwards through the faults of the Salt Wash Graben, or possibly via the Little Grand Wash Fault before moving southwards along the crest of the north-plunging Green River Anticline (Figure 8). The reducing fluids were trapped beneath the low-permeability topseal formed by the Earthy Member, into which there was long-term diffusion (Kampman et al., 2016). The reservoir was later breached by NNW-trending fractures related to extension across the crest of the Green River Anticline.

5.3 Distribution of the bleaching

5.3.1 Fold crest zone

Bleaching is seen within a broadly semi-circular area that is 1150 m across (parallel to the Salt Wash Graben Fault) and 408 m wide (perpendicular to the Salt Wash Graben Fault) on the crest of the Green River Anticline (Figure 1B). The upper contact between bleached (grey) with unbleached (red-brown) Entrada Sandstone is well exposed along the western and eastern exposed margins of the palaeoreservoir. Along the western margin, the grey-red contact is seen dipping toward the north from an elevation of around 1276 m to 1265 m. In the eastern part of the palaeoreservoir the contact climbs to an elevation of 1282 m toward the crest of the Green River Anticline (Figure 1B). Vertically, the zone of bleaching is at least 13 m thick, but its base is not seen and bleached sandstones are likely to extend into the concealed Slick Rock Member bedrock for an unknown depth (Figure 9). Neither is the full lateral extent of the bleaching known, because to the north it disappears into the subsurface beneath a cover of unbleached younger strata. The grey-red contact is undulating, irregular and locally cross-cuts the poorly-defined bedding within the Earthy Member. However, on the scale of the palaeoreservoir it is broadly conformable to the stratigraphy of the Entrada Sandstone, always occurring at a level just above the contact between the Slick Rock Member (permeable reservoir) and the Earthy Member (low permeability topseal). The vertical separation of the grey-red reduction front from the top of the Slick Rock Member typically ranges from 2 m to a maximum of 4 m. Changes in the thickness of the reduced zone are mostly smooth and undulating, but locally sharp where the boundary is offset by a fault or where the palaeoreservoir has been cut by secondary fractures and the reducing fluids have escaped vertically (Figure 9).

Within the Slick Rock reservoir lithofacies in this fold crest location the most notable aspect of the bleaching is its very uniform distribution and the way in which it crosses lithofacies boundaries (Figure 9A). The sedimentological differences between aeolian dune, wind-ripple and wavy-laminated sandstones do not appear to have had any influence on the migration of the reducing fluids. Within the palaeoreservoir only the well-cemented and relatively muddy wet interdune deposits show any tendency to remain (partially) unbleached suggesting that they probably acted as low permeability baffles (Figure 9B). Wet interdune deposits have laboratory measured permeabilities in the order of 0.1-1 mD and the ingress of reducing fluids would probably have been by a slow diffusion process (Kampman et al., 2016). Weakly cemented, clean aeolian sandstones have permeabilities in the order of 1000-10000 mD and would have acted as relatively rapid flow paths through the reservoir.

5.3.2 Fold flank zone

In locations off the crest of the Green River Anticline the bleaching of the Entrada Sandstone is less extensive. Figure 3 illustrates a typical example located on the eastern limb of the anticline where bleaching is localised within the uppermost 2-4 m of the Slick Rock Member. In contrast to the main palaeoreservoir on the fold crest, the bleaching does not extend for more than a few decimetres into the topseal formed by the Earthy Member. Bleaching is concentrated in high permeability, high angle cross-bedded aeolian dune deposits with limited penetration into intervening beds composed of low angle laminated dune apron deposits or muddy, wavy laminated interdune deposits.

6 Numerical modelling

6.1 Justification for numerical modelling

Many authors have studied the Entrada Sandstone bleached palaeoreservoirs around Green River in connection with CO_2 storage (Bickle et al., 2013; Kampman et al., 2016 and Dockrill and Shipton, 2010). However, thus far, there has been no attempt to construct a reservoir scale flow model to try and replicate the observed patterns of bleaching, an outcrop proxy for the distribution of CO_2-charged reducing-fluids. The modelling described below has two main objectives, first to investigate the regional pathways for the ingress of buoyant CO_2-charged fluids into the reservoir and second, to examine the influence of heterogeneity at lithofacies scale.

6.2 Model description

A simplified geological model was constructed in Petrel (Schlumberger, 2016) that captures the essential observed geometry of the palaeoreservoir as a NNW plunging anticline with updip closure against a fault (Figure 10). The palaeoreservoir (Slick Rock Member of the

Entrada Sandstone) was subdivided into dipping facies each with a thickness of around 5 m. The facies replicate, in a highly simplified way, the characteristic stacked beds of wet interdune, damp interdune and aeolian dune deposits within the Slick Rock Member, with each facies assigned a permeability of 10, 100, and 1000 mD and a porosity of 5, 15, and 25% respectively. Permeability anisotropy of 0.1 was assumed for the reservoir. The permeability and porosity of the Earthy Member of Entrada Sandstone, which acted as a topseal, was set to be 0.1 mD and 0.01%, respectively. The reservoir and topseal properties used in the model are summarised in Table 2.

The grid for the dynamic flow model had dimensions of 1500× 2000× 90 m and was discretized into 225,000 active cells (ni=75 nj=100 nk=30). The grid spacing was uniform in x and y direction throughout the model. Grid spacing in z direction is uniform throughout the reservoir and non-uniform in the caprock. The simulations were performed using ECLIPSE 300 compositional simulator with the CO2STORE option (Schlumberger, 2017). The bleaching fluid was a low temperature (approximately 27 °C) CO_2-saturated brine with a salinity around 2.5-7.0 wt% (Wigley et al., 2012; Bodnar, 2003). As such, it is assumed that the bleaching occurred at a depth shallower than the probable maximum burial depth (2.5 km). Hence, the depth was set to at 1 km with CO_2 in a supercritical state.

To predict the fate of injected CO_2 in the reservoir, numerical models need information on the relative permeability and capillary pressure of CO_2-brine system (Bennion and Bachu 2005). The experimental data on these two parameters are scarce, therefore, empirical formulations have been used to construct the capillary pressure (Pc), saturation (S), and relative permeability (kr) relationship (Pc–S–kr relationship). To generate the Pc–S–kr relationships, numerical modelling studies have generally assumed the generic value for the pore size index typical of sedimentary reservoir targeted for CO_2 storage (e.g. Rutqvist et al. 2008; Birkholzer et al. 2009; Oostrom et al. 2016). This value is considered constant for the entire storage formation regardless of the geological heterogeneity of the model. This assumption ignores variation in the average pore size of rock lithologies within layers in the reservoir and since flow processes greatly depend on the Pc–S–kr relationship, the accuracy of the simulation results is jeopardized (Onoja and Shariatipour, 2018). Here, drainage and imbibition relative permeability and capillary pressure curves for different lithologies are from Onoja et al. (2019) and Onoja and Shariatipour (2018). They studied the effect of sediment-size variation and showed that the existence of sediment gradation has an important effect on CO_2 migration. Drainage relative permeability curves and capillary pressure curves used in this study are shown in Figure 11(a) and (b).

Flow distribution was modelled under an isothermal condition of 27 °C and an initial pressure of 100 bar at 1000 m depth with the hydrostatic gradient of 10 bar/m. Initially, it was assumed that the reservoir contained 100% brine, with the mole fraction of 0.98 and 0.02 for water and NaCl, respectively.

To maintain the geomechanical stability and avoid damage to the reservoir, the pressure needs to remain below 80% of lithostatic pressure at any point within the model (USEPA, 1994; Breckels and van Eekelen, 1982). Fracture pressure gradient varies from 0.108 to 205 bar/m in different regions in the United States. Generally, however, 0.18 bar/m fracture pressure is used and it is assumed that this value is sufficient for this study. The wells were controlled by the surface rate with a maximum pressure limit of 200 bar. During simulation studies, the pressure did not reach the pressure constraint. CO_2 was injected for 20 years followed by 1000 post-injection period to study the CO_2 plume migration.

6.3 Modelling to test regional flow pathways

6.3.1 Model configuration

The pathway for the ingress of buoyant reducing fluid into the bleached Entrada Sandstone palaeoreservoir is still uncertain, with possible routes into the crest of the plunging Green River Anticline via the northern bounding fault of the Salt Wash Graben and the Little Grand Wash Fault further to the north (Figure 8). Numerical simulations were conducted to investigate which of these two major faults was the more likely pathway. To do so, three models were considered. In Model 1, a CO_2 injector well was completed on the left-side of the 3D model (southern-end) to simulate a pathway for reducing fluid from the northern fault of Salt Wash Graben. In Model 2, CO_2 was injected from the right-hand side of the 3D model (northern-end) of the model to simulate a source of CO_2 from the Little Grand Wash Fault. The injection rate was 4000 sm^3/day in these two models. In another study (Model 3), it was assumed that both of these two major faults were involved in the bleaching by placing two injector wells on both sides of the model (both northern and southern end of the 3D model).

The injection rate was 8000 sm^3/day in Model 3 (4000 sm^3/day for each well). In all these three models CO_2 was injected through completion from the uppermost high-permeability layer (Table 3). The primary justification for this injection point is field evidence that shows the localisation of bleaching in the uppermost high-permeability sandstone just below the caprock in areas that lie on the flanks of the palaeoreservoir (Figure 3). These uppermost high-permeability layers are therefore likely to have formed pathways for buoyant reducing fluids into the reservoir. The transmissibility of the faults was assumed to be 0 in j direction which was complete lateral barrier to flow.

6.3.2 Model results

The first model tested the hypothesis that the palaeoreservoir was filled via the northern bounding fault of Salt Wash Graben, with CO_2 injected from the left-hand side of the model (Figure 12). During the injection period, the simulation results demonstrate that, due to injection pressure, CO_2 migrated laterally through the uppermost high-permeability layer near the injection well and also migrated into the base of the topseal (Figure 12a). However, in the subsequent shut-in period (Figure 12b), CO_2 moved upward under buoyancy, migrated through the low-permeability Earthy Member topseal, and ultimately may reach the surface. At the end of the simulation study, it is observed that CO_2 mainly migrated vertically through the imperfect seal rather than downdip through high permeability lithofacies. Figure 13 provides the front (a) and top view (b) of the CO_2 mole fraction at the end of the simulation and shows that CO_2 migration was limited to the area near the injection well. Overall this model does not appear to be a close match to the distribution of bleaching seen in the palaeoreservoir, which extends over a considerably larger area for at least 1150 m parallel to the Salt Wash Graben and 408 m wide perpendicular to the Salt Wash Graben Fault (Figure 1B).

In the second model, CO_2 was injected through the uppermost high permeability layer of the Slick Rock reservoir from the northern boundary of the model, simulating that the main pathway for CO_2 which was the Little Grand Wash Fault. The injection location was thus downdip from the palaeoreservoir on the northern part of the north-plunging Green River Anticline. Figure 14 shows the CO_2 mole fraction during the injection period (a) and CO_2 mole fraction post-injection period (b). During the injection period, CO_2, migrated up-dip away from the well through the high-permeability carrier bed due to buoyancy forces and diffused into a bottom part of the topseal. After 20 years, the injection was stopped and the simulation was continued for 1000 years. During this period, CO_2 continued to migrate up dip through both

Slick Rock Member and base of Earthy Member of the Entrada Sandstone. Depending on injection rates, CO_2 might reach the other side of the model which is impervious to flow. Figure 15 illustrates the front view (a) and top view (b) of CO_2 mole fraction when CO_2 was injected from a down-dip location on the Little Grand Wash Fault. In this case, the flow was distributed across a broader area than what had been observed from injection via the northern bounding fault of the Salt Wash Graben. The model appears to be a closer match to the observed distribution of bleaching in the palaeoreservoir in particular, (1) the broad area of bleaching observed within the main reservoir zone on the anticlinal crest (Figure 1B), (2) the greater penetration of bleaching into the topseal in the main fold-crest reservoir (see Figure 9), (3) the general localisation of flow within high-permeability carrier beds in parts of the reservoir distant from the fold crest (see Figure 3). A primary source of CO_2-charged reducing fluids from the Little Grand Wash Fault also matches with the observations of Dockrill and Shipton (2010) that along this fault travertine deposits are particularly thick and well-developed, while those along the Salt Wash Graben are less well-developed and thinner.

It is also possible that both faults were involved in routing CO_2-charged reducing fluids into the palaeoreservoir and this scenario was explored in a third model. Figure 16 illustrates CO_2 mole fraction of this study at the end of simulation studies. The results show the combined characteristics of the previous model runs with nothing to indicate that this scenario could not have produced the observed patterns of bleaching. The main conclusion from the modelling remains, however, that some component of updip migration of CO_2-charged fluids from the Little Grand Wash Fault to the north was required to produce the observed patterns of bleaching.

6.4 Modelling to test the impact of reservoir heterogeneity

6.4.1 Model configuration

To further test the impact of reservoir heterogeneity two models were compared. Model A was configured as previously described and shown in Figure 10 with facies varying in permeability across four orders of magnitude up to a maximum value of 1000 mD. To account for the possibility of higher permeability values for aeolian sandstones, Model B was modified to include facies with a permeability range across six orders of magnitude up to a maximum of 10000 mD.

6.4.2 Model results

Both models displayed the uniform and widespread distribution of injected CO_2 which is consistent with the observed distribution of bleaching (Figure 17). Figure 23 plots the amount of dissolved CO_2 against time in the two models and shows that CO_2 dissolution is significantly higher in Model B than Model A during the injection period. This is because the layer with the high permeability of 10,000 mD allowed for faster migration of CO_2. As such, CO_2 covered a broader area in a shorter period of time. Therefore in Model B, CO_2 was in more contact with formation brine causing more CO_2 dissolution (around 42%). However, at the end of simulation study, CO_2 swept uniformly across all lithofacies boundaries with different permeability values resulting in an equal total amount of CO_2 dissolution in the brine of the two models.

7 Discussion

The bleached sandstone palaeoreservoirs of the Colorado Plateau have seen a resurgence of interest in recent years as analogues for the types of subsurface geological formations that might be used as storage of CO_2 as part of CCS schemes (Bickle et al., 2013). Relative to subsurface geological investigations, the study of exhumed CO_2 palaeoreservoirs is low cost and provides a uniquely immersive view of how migrating fluids have interacted with the geological matrix and rock fractures.

The main hypothesis of this study was that the highly heterogeneous character of the Entrada Sandstone (typical of a ‘wet aeolian’ depositional system) should have had a major impact on the distribution of the CO_2 charged reducing fluids and thus the distribution of bleaching. The results of the study showed, however, that within the palaeoreservoir lithofacies boundaries and heterogeneity had relatively little control on the distribution of bleaching even though these extended across large permeability ranges of at least three orders of magnitude. Flow simulations on simplified models of the Entrada Sandstone palaeoreservoirs confirm the outcrop observations with relatively little confinement of injected CO_2 within layers of highly contrasting permeability. The study shows the potential for relatively uniform distribution of injected CO_2 even where considerable heterogeneity and permeability contrasts exist within the target formation.

It is important here to consider the nature of the invasive fluids, and at Salt Wash Graben these are likely to have been relatively low viscosity brines with CO_2 and CH_4 (Wigley et al., 2013) rather than a high viscosity fluid such as oil. The results of our study would thus appear to provide some validation of Flora's Rule (Ringrose and Bentley, 2015). 'Flora's Rule' is general rule of thumb that has its foundation in the viscosity term in the Darcy flow equation and states that while viscous fluids such as oil might be sensitive to one or two orders of permeability variation for a given porosity class, gas reservoirs might only be sensitive to three orders of magnitude. This appears to have been broadly the case for the Entrada Sandstone palaeoreservoir at Salt Wash Graben where the bleaching is uniform across the majority of lithofacies boundaries. This rule has important practical significance in understanding how much sedimentological information needs to be incorporated into reservoir models: which is likely to be considerably less where the fluids under consideration are of low viscosity (Bentley and Ringrose, 2018). Sedimentologists often expend considerable time subdividing reservoirs and aquifers into numerous lithofacies and incorporating these into complex static models. The widespread distribution of bleaching within this palaeoreservoir suggests this information may not be required to achieve a realistic simulation.

However, the apparent lack of spatial correlation between fluid migration, bleaching and lithofacies with high permeability contrasts is likely to be strongly dependent on the residence time and pressure of reducing fluids within the reservoir. Where the residence time is short and pressures are low the permeability of lithofacies is likely to play an increasingly important role on determining fluid movement. This is clearly illustrated by the outcrop. Bleached outcrops of the Entrada Sandstone that are located outside the main crestal palaeoreservoir on the flanks of the Green River Anticline show that bleaching is concentrated in highpermeability aeolian dune cross-strata with relatively little penetration into adjacent lower permeability lithofacies. Both the outcrop and the flow simulation indicate that an understanding of lithofacies variation is thus critical for understanding pathways and areas of transient flow. Only when the permanent trap is reached will the importance of lithofacies variation on the long-term distribution of fluids start to be reduced.

8 Conclusions

One of the primary aims of this study has been to show that exhumed bleached palaeoreservoirs provide a useful and (relative to subsurface studies) low cost means of understanding large-scale patterns of fluid flow in geological media. The phenomenon of bleaching, where the former presence and movement of reducing fluids is captured as visible mineralogical and geochemical changes in early-diagenetically reddened rock, greatly increases the value of 'conventional' outcrop analogue studies in relation to the subsurface storage of CO_2. Outcrop provides information on geological heterogeneity at a scale that bridges the gap between data from well core and seismic reflection. Careful matching of proposed subsurface geological stores of CO_2 with comparable bleached palaeoreservoir analogues could be an important means of gaining additional insight into the long-term fate of stored $CO_{2,}$ particularly when outcrop studies are augmented by flow modelling.

The study has focussed on the Entrada Sandstone in SE Utah: a classic example of a wet aeolian deposition system, where complex metre-scale layered heterogeneity is produced by the migration and accretion of aeolian dune and wet interdune deposits. The Entrada Sandstone is potentially a useful analogue for comparable continental red-bed formations that are under consideration as geological storage for CO_2 on the NW European continental shelf. On the Colorado Plateau the Entrada Sandstone has been extensively bleached by migrating CO_2 charged reducing fluids providing an opportunity to examine how such fluids migrate and accumulate within these heterogeneous aeolian deposits.

Examination of a bleached palaeoreservoir within the Entrada Sandstone has shown that, despite the geological heterogeneity and strong permeability contrasts, the distribution of bleaching is remarkably uniform. A key conclusion is therefore that, given sufficient residence time, geological heterogeneity within the range 1-10^3 md should not greatly impede the relatively uniform distribution of CO_2 charged fluids throughout a reservoir. This conclusion has been substantiated here by flow modelling. However, where flows are transient fluid movement will be focussed along high-permeability pathways, as also evidenced by modelling and the localisation of bleaching within aeolian dune lithofacies on the flanks of anticlinal trap described at Salt Wash Graben.

The Entrada Sandstone palaeoreservoir at Salt Wash Graben has been the subject of much recent CCS related research. This study shows the reservoir is located on the crest of the north-plunging Green River Anticline with an updip seal formed by downfaulted mudstone-rich Cedar Mountain Formation in the Salt Wash Graben. Flow modelling indicates that the most likely source of the CO_2 charged reducing fluids was the Little Grand Wash Fault to the north with updip migration into the reservoir.

Acknowledgements

AJN and ASB publish by permission of the Executive Director, British Geological Survey.

9 References

AGRC, 2018. Utah Automated Geographic Reference Centre. https://gis.utah.gov/.

Allis, R., Chidsey, T., Gwynn, W., Morgan, C., White, S., Adams, M. and Moore, J., 2001, May. Natural CO_2 reservoirs on the Colorado Plateau and southern Rocky Mountains: Candidates for CO_2 sequestration. In Proceedings of the First National Conference on Carbon Sequestration (pp. 14-17). US Department of Energy, National Energy Technology Laboratory Washington, DC.

Baars, D.L., Doelling, H.H., 1987. Moab salt-intruded anticline, east-central Utah. In: S.S. Beus (Ed.), Geological Society of America Centennial Field Guide—Rocky Mountain Section, Centennial Field Guide Volume 2. Geologic Society of America, Boulder, Colorado, pp. 275-280.

Bachu, S. (2000) 'Sequestration of CO_2 in Geological Media: Criteria and Approach for Site Selection in Response to Climate Change'. Energy Conversion and Management 41 (9), 953-970

Bachu, S., 2008. CO_2 storage in geological media: Role, means, status and barriers to deployment. Progress in Energy and Combustion Science, 34(2), pp.254-273.

Beitler, B., Chan, M.A., Parry, W.T., 2003. Bleaching of Jurassic Navajo Sandstone on Colorado Plateau Laramide highs: Evidence of exhumed hydrocarbon supergiants? Geology, 31(12): 1041-1044.

Bennion, B. and Bachu, S., 2005, January. Relative permeability characteristics for supercritical CO_2 displacing water in a variety of potential sequestration zones. In SPE Annual Technical Conference and Exhibition. Society of Petroleum Engineers.

Bentley, M., Ringrose, P., 2018. Future directions in reservoir modelling: new tools and ‘fit-forpurpose’ workflows. Geological Society, London, Petroleum Geology Conference Series, 8(1): 537-546.

Bickle, M., Kampman, N., 2013. Lessons in carbon storage from geological analogues. Geology, 41(4): 525-526.

Bickle, M., Kampman, N., Wigley, M., 2013. Natural Analogues. Reviews in Mineralogy and Geochemistry, 77(1): 15-71.

Biddle, K.T. and Wielchowsky, C.C., 1994. Hydrocarbon Traps: Chapter 13: Part III. Processes.

Birkholzer J.T., Zhou Q., Tsang C.F. Large-scale impact of CO_2 storage in deep saline aquifers: A sensitivity study on pressure response in stratified systems. International Journal Greenhouse Gas Control. 2009;3(2):181–94.

Blakey, R.C., Peterson, F., Kocurek, G., 1988. Synthesis of late Paleozoic and Mesozoic eolian deposits of the Western Interior of the United States. Sedimentary Geology, 56(1–4): 3-125.

Bodnar, R.J., 2003. Introduction to aqueous-electrolyte fluid inclusions. Fluid inclusions: analysis and interpretation, 32, pp.81-100.

Breckels, I.M. and Van Eekelen, H.A.M., 1982. Relationship between horizontal stress and depth in sedimentary basins. Journal of Petroleum Technology, 34(09), pp.2-191.

Bristow, C., Mountney, N.P., 2013. Aeolian Stratigraphy. In: J.F. Shroder (Ed.), Treatise on Geomorphology. Academic Press, San Diego, pp. 246-268.

Burnside, N.M., Shipton, Z.K., Dockrill, B., Ellam, R.M., 2013. Man-made versus natural CO_2 leakage: A 400 k.y. history of an analogue for engineered geological storage of CO_2. Geology.

Chan, M.A., Parry, W.T., Bowman, J.R., 2000. Diagenetic Hematite and Manganese Oxides and FaultRelated Fluid Flow in Jurassic Sandstones, Southeastern Utah. AAPG Bulletin, 84(9): 1281-1310.

Crabaugh, M., Kocurek, G., 1993. Entrada Sandstone: an example of a wet aeolian system. Geological Society, London, Special Publications, 72(1): 103-126.

Craddock, W.H., Blondes, M.S., DeVera, C.A., Hunt, A.G., 2017. Mantle and crustal gases of the Colorado Plateau: Geochemistry, sources, and migration pathways. Geochimica et Cosmochimica Acta, 213: 346-374.

Dockrill, B., Shipton, Z.K., 2010. Structural controls on leakage from a natural CO_2 geologic storage site: Central Utah, U.S.A. Journal of Structural Geology, 32(11): 1768-1782.

Doelling, H.H., 2001. Geologic map of the Moab and eastern part of the San Rafael Desert 30' x 60' quadrangles, Grand and Emery Counties, Utah, and Mesa County, Colorado. Utah Geological Survey, Map 180, 1:100000, Map 180. Utah Geological Survey.

Duan, Z. and Sun, R., 2003. An improved model calculating CO_2 solubility in pure water and aqueous NaCl solutions from 273 to 533 K and from 0 to 2000 bar. Chemical geology, 193(3-4), pp.257-271.

Ennis-King, J. and Paterson, L., 2002, January. Engineering aspects of geological sequestration of carbon dioxide. In SPE Asia Pacific Oil and Gas Conference and Exhibition. Society of Petroleum Engineers.

Ge, H., Jackson, M.P.A., 1998. Physical modeling of structures formed by salt withdrawal; implications for deformation caused by salt dissolution. AAPG Bulletin, 82(2): 228-250.

Goodall, T.M., North, C.P., Glennie, K.W., 2000. Surface and subsurface sedimentary structures produced by salt crusts. Sedimentology, 47(1): 99-118.

Han, W.S. et al., 2013. Characteristics of CO_2-driven cold-water geyser, Crystal Geyser in Utah: experimental observation and mechanism analyses. Geofluids, 13(3): 283-297.

Haszeldine, R., S. et al., 2005. Analogues géochimiques naturels pour le stockage du dioxyde de carbone en réservoir géologique poreux profond : perspective pour le Royaume-Uni. Oil & Gas Science and Technology - Rev. IFP, 60(1): 33-49.

Howell, J.A., Martinius, A.W., Good, T.R., 2014. The application of outcrop analogues in geological modelling: a review, present status and future outlook. Geological Society, London, Special Publications, 387.

IPCC, (2005) IPCC Special Report on Carbon Dioxide Capture and Storage. In: METZ, B., DAVIDSON, O., DE CONINCK H.C., LOOS, M., MEYER, L.A. (Eds.), Prepared by Working Group III of the Intergovernmental Panel on Climate Change. Cambridge University Press, Cambridge, UK/New York, NY, USA, 442 pp.

Kampman, N. et al., 2012. Pulses of carbon dioxide emissions from intracrustal faults following climatic warming. Nature Geosci, 5(5): 352-358.

Kampman, N. et al., 2016. Observational evidence confirms modelling of the long-term integrity of CO_2-reservoir caprocks. Nature Communications, 7: 12268.

Kampman, N. et al., 2013. Scientific drilling and downhole fluid sampling of a natural CO_2 reservoir, Green River, Utah. Sci. Dril., 16: 33-43.

Kocurek, G., 1981. Erg reconstruction: The Entrada Sandstone (Jurassic) of northern Utah and Colorado. Palaeogeography, Palaeoclimatology, Palaeoecology, 36(1–2): 125-153.

Kocurek, G., Fielder, G., 1982. Adhesion structures. Journal of Sedimentary Research, 52(4): 12291241.

Lu, J., Kordi, M., Hovorka, S.D., Meckel, T.A. and Christopher, C.A., 2013. Reservoir characterization and complications for trapping mechanisms at Cranfield CO_2 injection site. International Journal of Greenhouse Gas Control, 18, pp.361-374.

Newell, A.J., Shariatipour, S.M., 2016. Linking outcrop analogue with flow simulation to reduce uncertainty in sub-surface carbon capture and storage: an example from the Sherwood Sandstone Group of the Wessex Basin, UK. Geological Society, London, Special Publications, 436.

Nordbotten, J.M., Celia, M.A. and Bachu, S., 2005. Injection and storage of CO_2 in deep saline aquifers: Analytical solution for CO_2 plume evolution during injection. Transport in Porous media, 58(3), pp.339360.

Nuccio, V.F., Condon, S.M., 1996. Burial and Thermal History of the Paradox Basin, Utah and Colorado, and Petroleum Potential of the Middle Pennsylvanian Paradox Formation. US Geological Survey, Bulletin 2000-O, 41p.

Ogata, K., Senger, K., Braathen, A., Tveranger, J., 2014. Fracture corridors as seal-bypass systems in siliciclastic reservoir-cap rock successions: Field-based insights from the Jurassic Entrada Formation (SE Utah, USA). Journal of Structural Geology, 66(0): 162-187.

Onoja, M.U., Ahmadinia, M., Shariatipour, S.M. and Wood, A.M., 2019. Characterising the role of parametric functions in the van Genuchten empirical model on CO2 storage performance. International Journal of Greenhouse Gas Control, 88, pp.233-250.

Onoja, M.U. and Shariatipour, S.M., 2018. The impact of gradational contact at the reservoir-seal interface on geological CO 2 storage capacity and security. International Journal of Greenhouse Gas Control, 72, pp.1-13.

Oostrom M., White M.D., Porse S.L., Krevor S.C.M., Mathias S.A. Comparison of relative permeabilitysaturation-capillary pressure models for simulation of reservoir CO_2 injection. International Journal of Greenhouse Gas Control. 2016;45:70–85.

Rutqvist J., Birkholzer J.T., Tsang C.F. Coupled reservoir-geomechanical analysis of the potential for tensile and shear failure associated with CO_2 injection in multilayered reservoir-caprock systems. Int J Rock Mech Min Sci. 2008;45(2):132–43.

Pearce, J.M. et al., 2011. Reservoir-scale CO_2-fluid rock interactions: Preliminary results from field investigations in the Paradox Basin, Southeast Utah. Energy Procedia, 4(0): 5058-5065.

Pentland, C.H., El-Maghraby, R., Iglauer, S. and Blunt, M.J., 2011. Measurements of the capillary trapping of super-critical carbon dioxide in Berea sandstone. Geophysical Research Letters, 38(6).

Pourmalek, A and Shariatipour, S.M, 2018. Dependence on temperature and salinity gradients and the injection rate of the CO2 storage in saline aquifers with an angular unconformity. *Journal of Porous Media* (in press). DOI.10.1615/JPorMedia.2019025077.

Pruess, K., 2006. On CO_2 Behavior in the Subsurface, Following Leakage from a Geologic Storage Reservoir.

Pruess, K., García, J., Kovscek, T., Oldenburg, C., Rutqvist, J., Steefel, C. and Xu, T., 2002. Intercomparison of numerical simulation codes for geologic disposal of CO_2.

Ringrose, P., Bentley, M., 2015. Reservoir Model Design: A Practitioner's Guide. Springer, Dordrecht, 249 pp.

Rushton, J.C., Wagner, D., Pearce, J.M., Rochelle, C.A., Purser, G., 2018. Red-bed bleaching in a CO_2 storage analogue: insights from Entrada Sandstone fracture-hosted mineralization. Journal of Sedimentary Research, in review.

Salvi, S., Quattrocchi, F., Brunori, C.A., Doumaz, F., Angelone, M., Billi, A., Buongiorno, F., Funiciello, R., Guerra, M., Mele, G. and Pizzino, L., 1999. A multidisciplinary approach to earthquake research: implementation of a Geochemical Geographic Information System for the Gargano site, Southern Italy. Natural Hazards, 20(2-3), pp.255-278.

Schumacher, D., 1996. Hydrocarbon-induced alteration of soils and sediments. In: D. Schumacher, M.A. Abrams (Eds.), Hydrocarbon migration and its nearsurface expression, pp. 71-89.

Sheldon, N.D., 2005. Do red beds indicate paleoclimatic conditions?: A Permian case study. Palaeogeography, Palaeoclimatology, Palaeoecology, 228(3–4): 305-319.

USEPA, 1994. Determination of maximum injection pressure for class i wells.

Walker, T.R., Waugh, B., Grone, A.J., 1978. Diagenesis in first-cycle desert alluvium of Cenozoic age, southwestern United States and northwestern Mexico. Geological Society of America Bulletin, 89(1): 19-32.

Wigley, M., Kampman, N., Chapman, H.J., Dubacq, B., Bickle, M.J., 2013. In situ redeposition of trace metals mobilized by CO_2-charged brines. Geochemistry, Geophysics, Geosystems, 14(5): 1321-1332.

Wigley, M., Kampman, N., Dubacq, B., Bickle, M., 2012. Fluid-mineral reactions and trace metal mobilization in an exhumed natural CO_2 reservoir, Green River, Utah. Geology.

Wright, J.C., Shawe, D.R., Lohman, S.W., 1962. Definition of members of Jurassic Entrada Sandstone in east-central Utah and west-central Colorado. AAPG Bulletin, 46(11): 2057-2070.

10 Figure Captions

Figure 1 (A) Map showing location of the study sites (black rectangles) adjacent to the Salt Wash Graben. Faults are shown in red, anticlinal axes in black and selected geological formations are coloured and labelled from Utah Geological Survey Map 180 (Doelling 2001). (B) Aerial photograph of the study site showing the conspicuous grey bleached area on the footwall of the northern bounding fault of the Salt Wash Graben. The bleached area (red line) largely corresponds to the Slick Rock Member (blue line) of the Entrada Sandstone but locally extends into the Earthy Member. Red stars indicate the location of the two logged sections in Figure 5.

Figure 2 Middle Jurassic stratigraphy and palaeogeography of Utah and western Colorado simplified from Blakey et al. (1988). Red star indicates the approximate stratigraphic and geographic position of the Salt Wash Graben site.

Figure 3 Representative examples of the Slick Rock and Earthy members of the Entrada Sandstone at Salt Wash Graben. This is outside of the main palaeoreservoir zone on the east flank of the Green River Anticline (see Figure 1A) but note patchy bleaching in the steeply dipping dune foresets that extends for a short distance into the overlying sandy siltstones of the Earthy Member.

Figure 4 View looking northwest along the northern bounding fault of the Salt Wash Graben showing the abrupt truncation of the Entrada Sandstone to the north against the Cedar

Mountain Formation to the south. Note extensive grey bleaching of the Slick Rock Member of the Entrada Sandstone that extends for several metres into the Earthy Member. Extensive tufa deposits result from expulsion of carbonate-rich water along the fault trace.

Figure 5 Logged sections through the upper parts of the Slick Rock Member and the lower parts of the Earthy Member of the Entrada Sandstone. Typical field-derived permeability values for each bed/lithofacies are shown in millidarcies (mD) plotted on a log scale. See Figure 1 for location of logged sections and Table 1 for key to lithofacies notation.

Figure 6 Illustration of the main sandstone lithofacies within the Slick Rock Member, (A) high angle cross-bedded dune sandstones, (B) low-angle wind-ripple laminated sandstone, (C) wavy and convolute laminated sandstone damp interdune deposits and (D) massive and muddy wet interdune sandstones. Permeability generally decreases from A-D.

Figure 7 (A) Field image of aeolian dune sandstone (Slick Rock Member) from USB microscope showing open pores, (B) SEM image of aeolian dune sandstone, (C) Field image of Earthy Member sandstone from USB microscope, (D) SEM image of Earthy Member showing porefilling calcite and dolomite cement.

Figure 8 Semi-schematic diagram showing two possible pathways for the migration of reducing fluids from depth into the Entrada Sandstone palaeoreservoir at Salt Wash Graben.

Figure 9 (A) West part of the palaeoreservoir showing bleached zone extending for around 4 m into the Earthy Member above the top of the Slick Rock Member (dotted white line). The horizontal grey-red contact is broadly concordant to the stratigraphy but above the boundary. Note fracture zone to the upper left (where fluids have escaped vertically following breaching of the topseal) and the very uniform distribution of bleaching within the Slick Rock Member. (B) East part of the palaeoreservoir showing (1) the relatively uniform distribution of bleaching within the Slick Rock Member, (2) the undulating reduction front several metres above the base of the Earthy Member, (3) bleached fractures developed following breaching of the topseal, and (4) the presence of red (unbleached) wet interdune deposits (white arrows) within the Slick Rock Member.

Figure 10 Reservoir model showing the distribution of lithofacies (Table 2) used for Eclipse simulations. Little Grand Wash (LGW) is placed at the right-end of the model and the northern fault of Salt Wash Graben (SWG) is placed at the left-hand side of the model.

Figure 11: (a) Drainage relative permeability curve and (b) Drainage capillary pressure curve for facies 1 (sandstone), facies 2 (silty sandstone), facies 3 (muddy sandstone) and facies 4 (sandy siltstone).

Figure 12 CO_2 mole fraction at the end of injection period (20 years) (a) and at the end of post-injection period (1000 years) (b) when CO_2 was injected from the left-hand side of the model.

Figure 13 Front view (a) and top view (b) of the CO_2 mole fraction at the end of the simulation when CO_2 was injected from the left-hand side of the model.

Figure 14 CO_2 mole fraction at the end of injection period (20 years) (a) and at the end of postinjection period (1000 years) (b) when CO_2 was injected from the right-hand side of the model.

Figure 15 Front view (a) and top view (b) of CO_2 mole fraction when CO_2 was injected from the right-hand side of the model.

Figure 16 CO_2 mole fraction in Model 3 when CO_2 was injected from both sides of the model.

Figure 17 (a) Distribution of CO_2 in the model with lithofacies set at a permeability range across four orders of magnitude (Model A in Table 4). (b) Distribution of CO_2 in the model with lithofacies set at a permeability range of six orders of magnitude (Model B in Table 4). Both scenarios result in a relatively uniform distribution of CO_2 that cross the boundaries of interlayered lithofacies (see Figure 15).

Figure 18 Total amount of CO_2 dissolution in the brine in Model A and Model B.

FIGURE 1

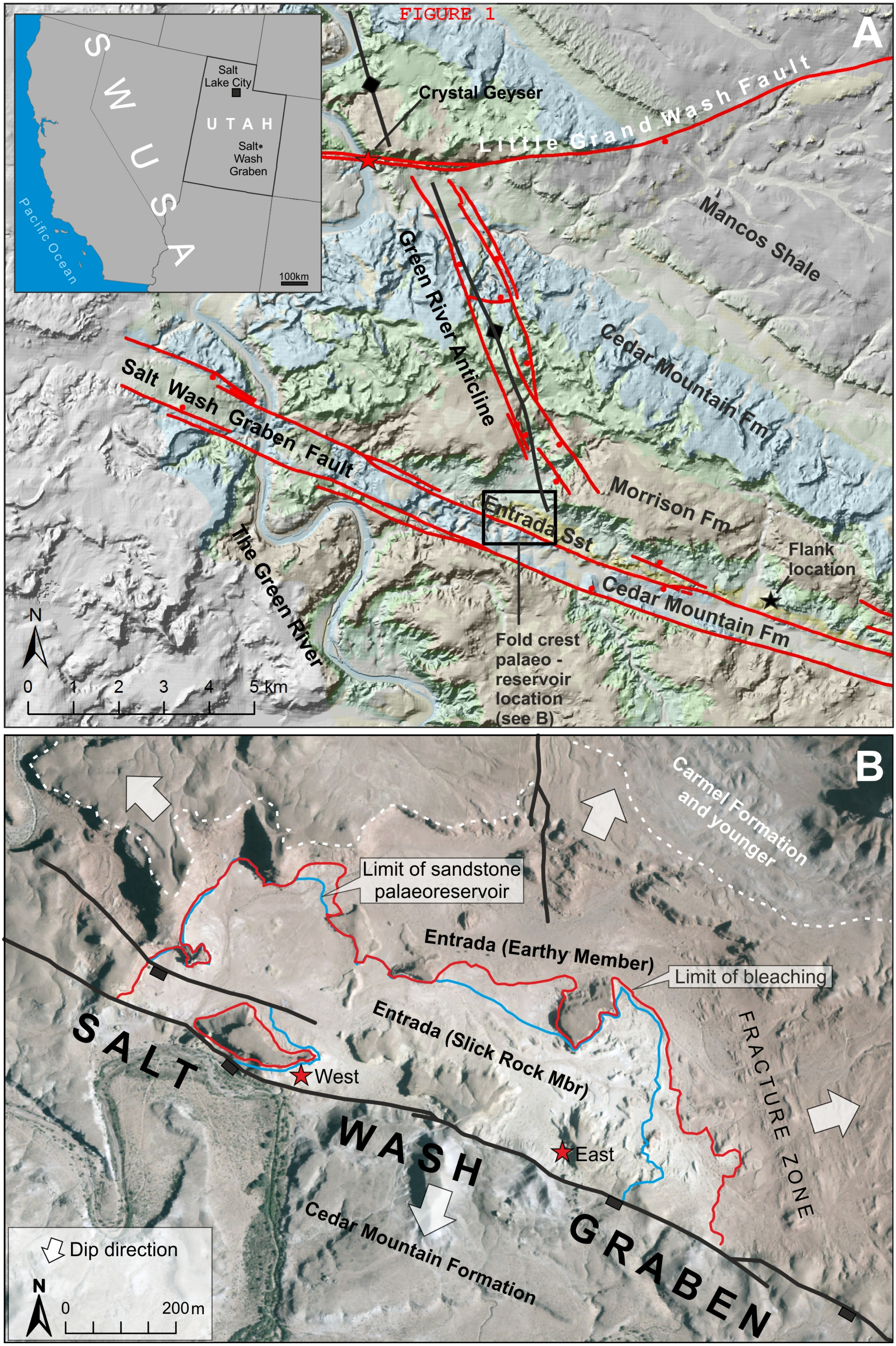
A
S W U S A
Salt Lake City
U T A H
Salt Wash Graben
Pacific Ocean
100km
Crystal Geyser
Little Grand Wash Fault
Mancos Shale
Green River Anticline
Cedar Mountain Fm
Salt Wash Graben Fault
Morrison Fm
Entrada Sst
Flank location
Cedar Mountain Fm
The Green River
Fold crest palaeo - reservoir location (see B)
N
0 1 2 3 4 5 km
B
Carmel Formation and younger
Limit of sandstone palaeoreservoir
Entrada (Earthy Member)
Limit of bleaching
Entrada (Slick Rock Mbr)
FRACTURE ZONE
West
East
SALT WASH GRABEN
Cedar Mountain Formation
Dip direction
N
0 200 m

FIGURE 2

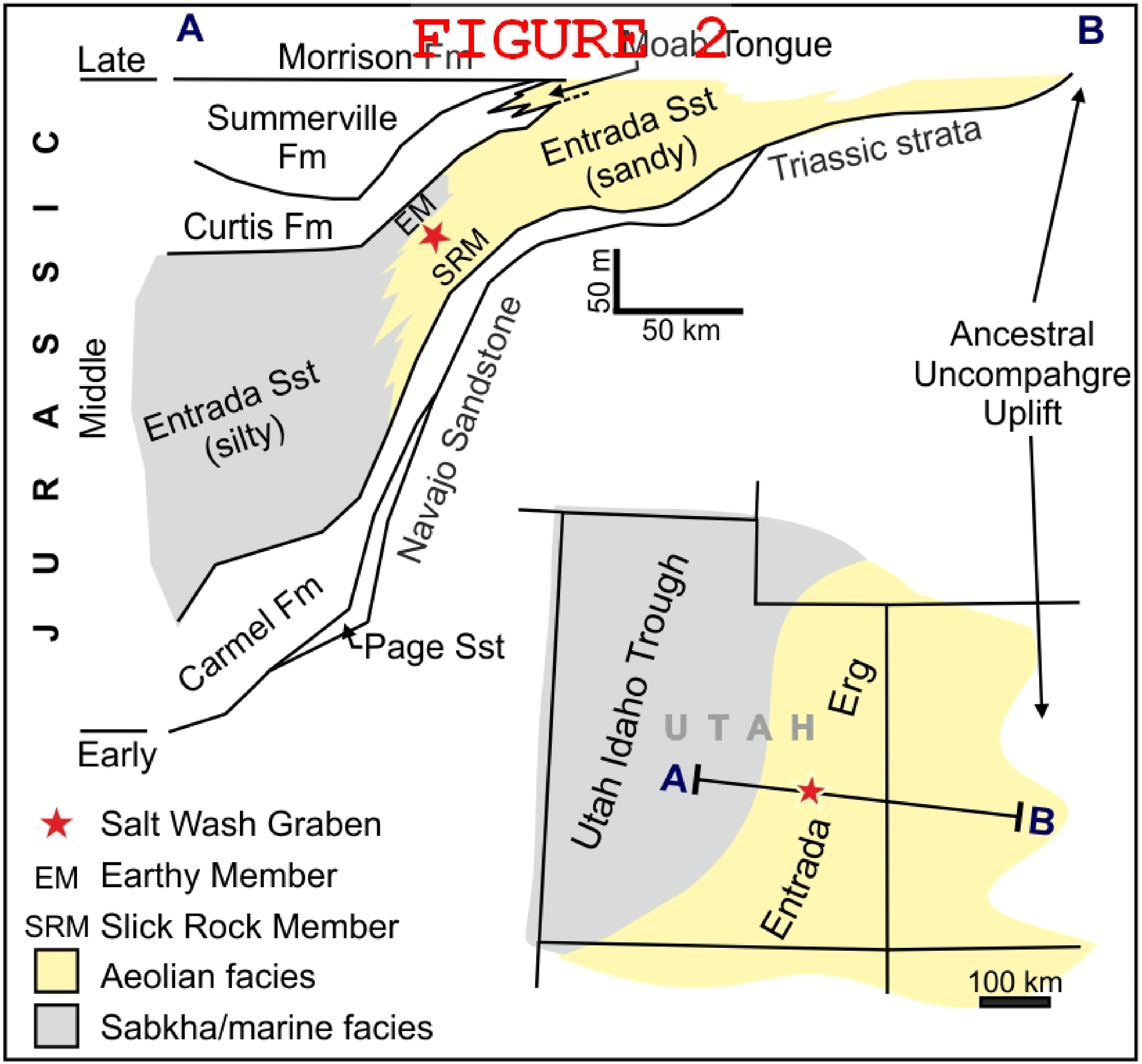
A
B
Late
Morrison Fm
Moab Tongue
Summerville Fm
Entrada Sst (sandy)
Triassic strata
Curtis Fm
EM
SRM
J U R A S S I C
Middle
Entrada Sst (silty)
Navajo Sandstone
50 m
50 km
Ancestral Uncompahgre Uplift
Carmel Fm
Page Sst
Early
Utah Idaho Trough
U T A H
Erg
Entrada
A
B
100 km
Salt Wash Graben
EM Earthy Member
SRM Slick Rock Member
Aeolian facies
Sabkha/marine facies

FIGURE 3

FIGURE 4

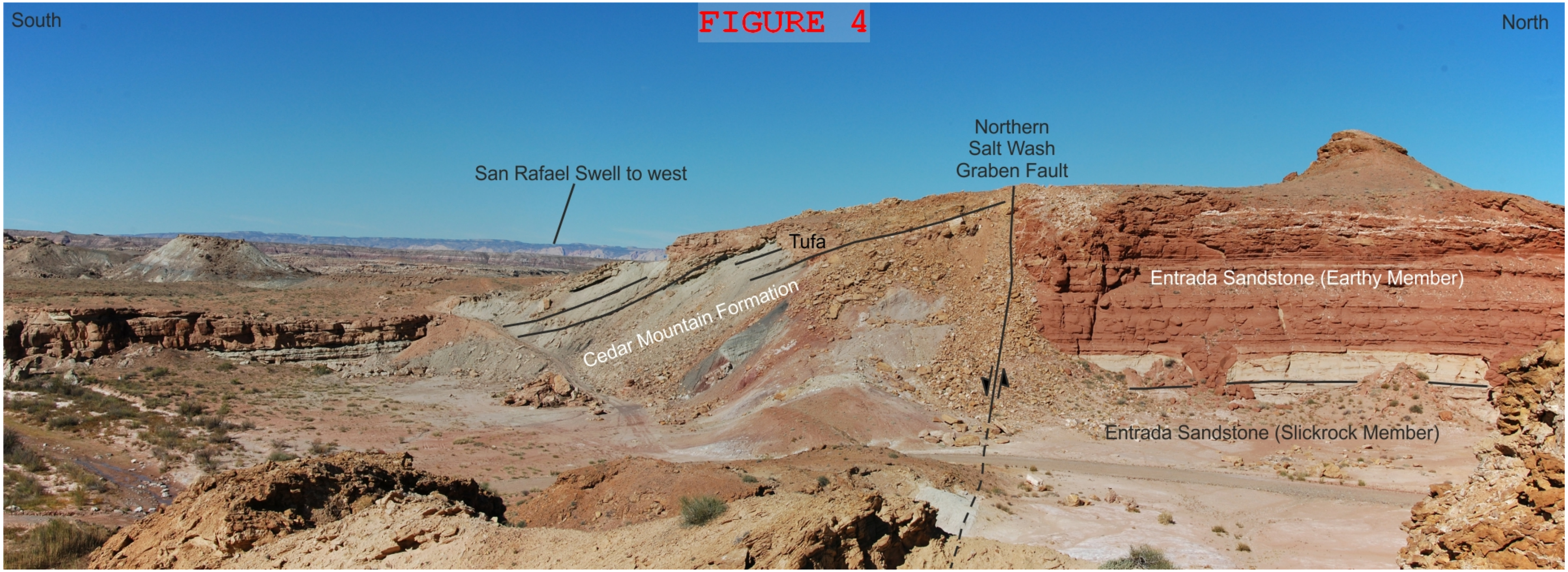
South
North
San Rafael Swell to west
Northern
Salt Wash
Graben Fault
Tufa
Cedar Mountain Formation
Entrada Sandstone (Earthy Member)
Entrada Sandstone (Slickrock Member)

FIGURE 5

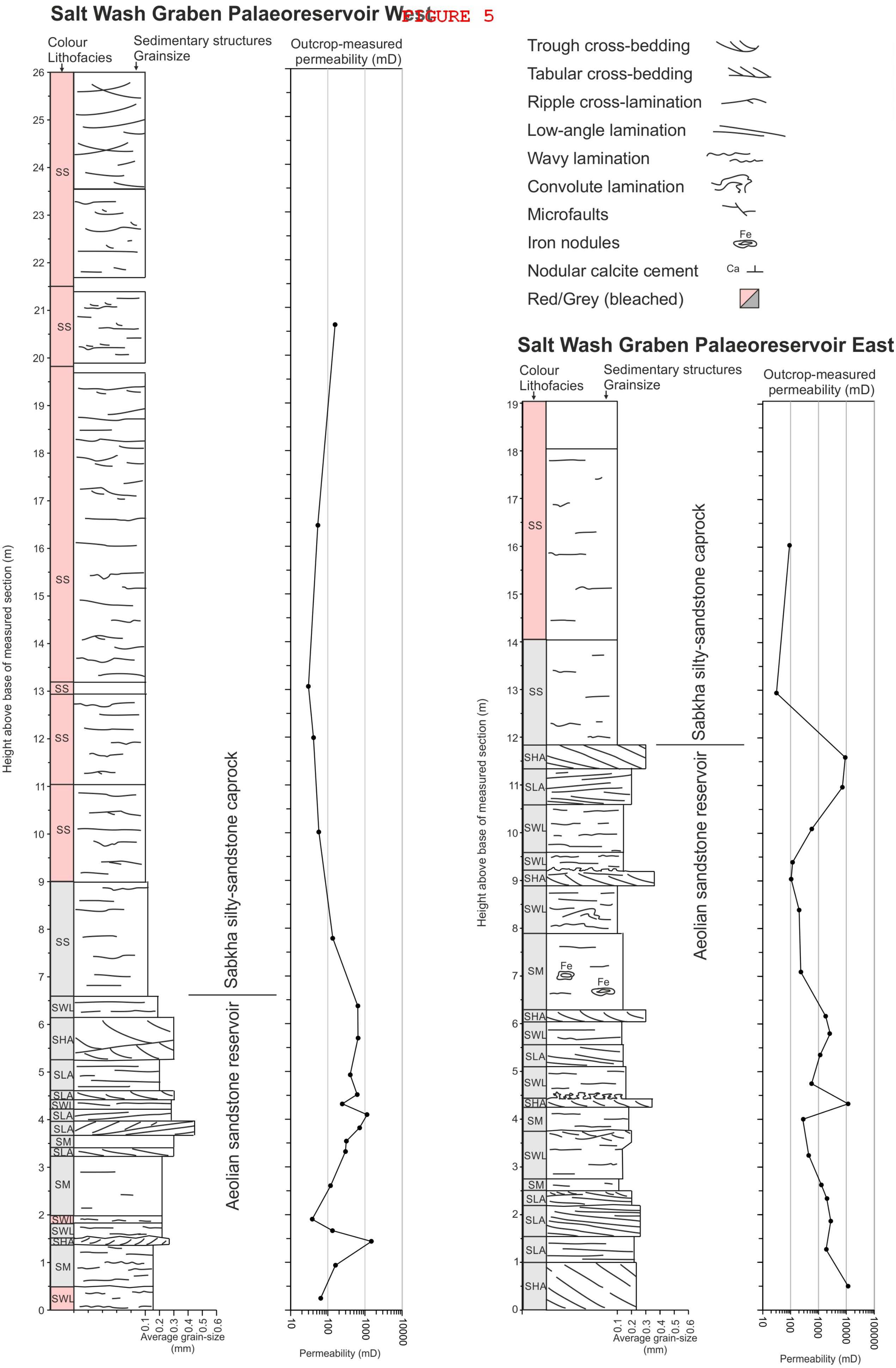
Salt Wash Graben Palaeoreservoir West
Colour
Lithofacies
Sedimentary structures
Grainsize
Outcrop-measured permeability (mD)
Height above base of measured section (m)
SS
SWL
SHA
SLA
SWI
SM
Sabkha silty-sandstone caprock
Aeolian sandstone reservoir
Average grain-size (mm)
Permeability (mD)
Trough cross-bedding
Tabular cross-bedding
Ripple cross-lamination
Low-angle lamination
Wavy lamination
Convolute lamination
Microfaults
Iron nodules
Fe
Nodular calcite cement
Ca
Red/Grey (bleached)
Salt Wash Graben Palaeoreservoir East
Colour
Lithofacies
Sedimentary structures
Grainsize
Outcrop-measured permeability (mD)
Height above base of measured section (m)
Sabkha silty-sandstone caprock
Aeolian sandstone reservoir
Average grain-size (mm)
Permeability (mD)

FIGURE 6

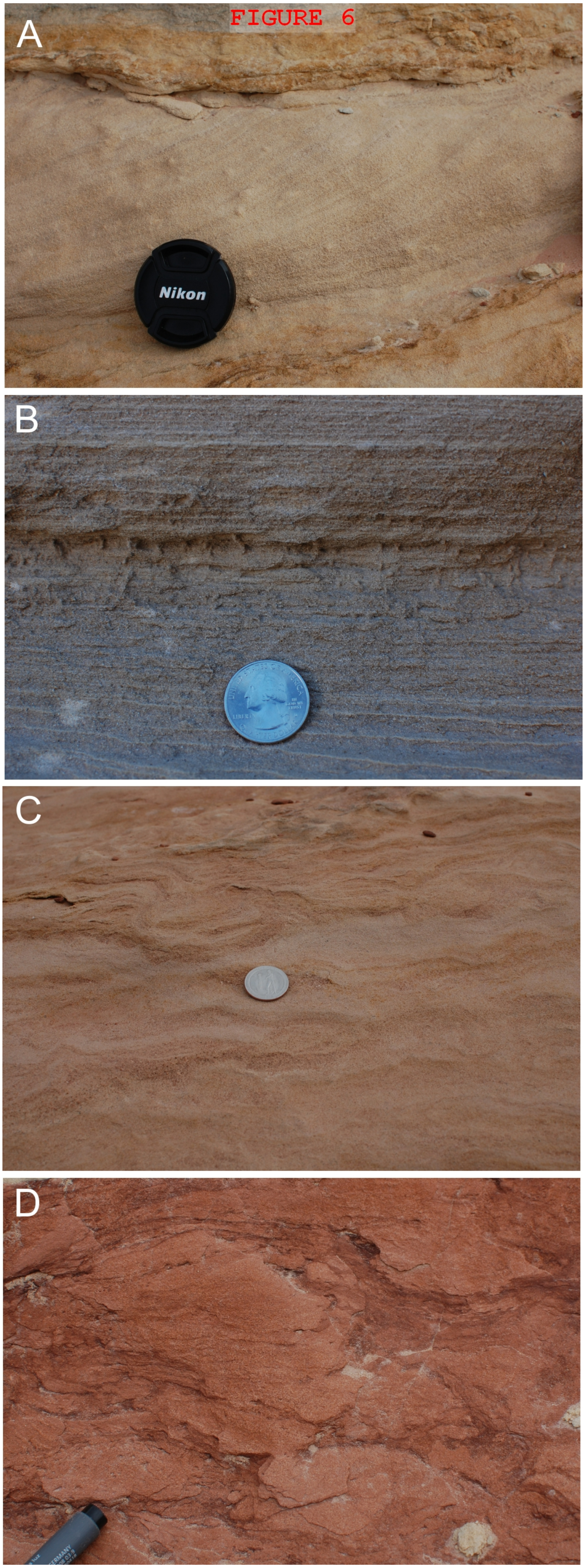

FIGURE 7

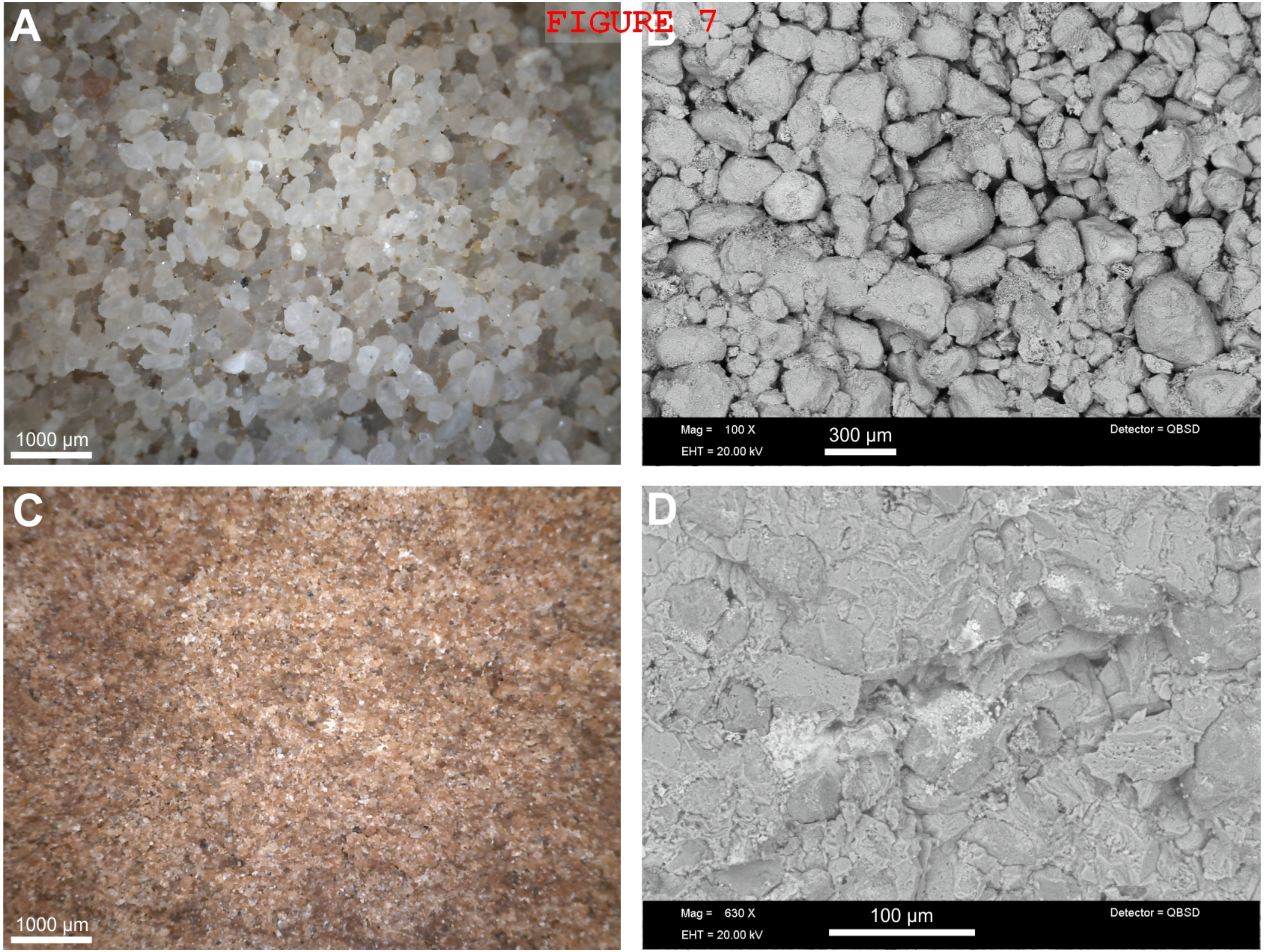
A
1000 µm
B
Mag = 100 X
EHT = 20.00 kV
300 µm
Detector = QBSD
C
1000 µm
D
Mag = 630 X
EHT = 20.00 kV
100 µm
Detector = QBSD

FIGURE 8

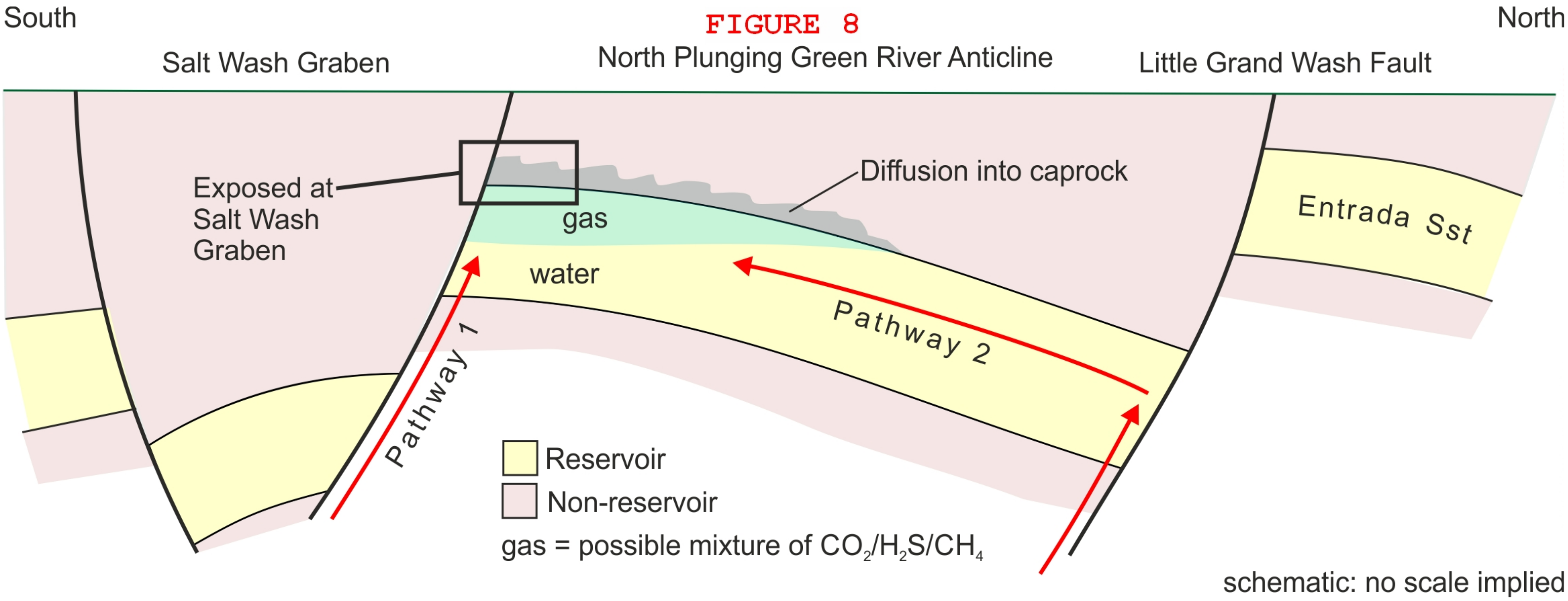
South
Salt Wash Graben
North Plunging Green River Anticline
Little Grand Wash Fault
North
Exposed at Salt Wash Graben
Diffusion into caprock
gas
water
Entrada Sst
Pathway 1
Pathway 2
Reservoir
Non-reservoir
gas = possible mixture of $CO_2/H_2S/CH_4$
schematic: no scale implied

FIGURE 9

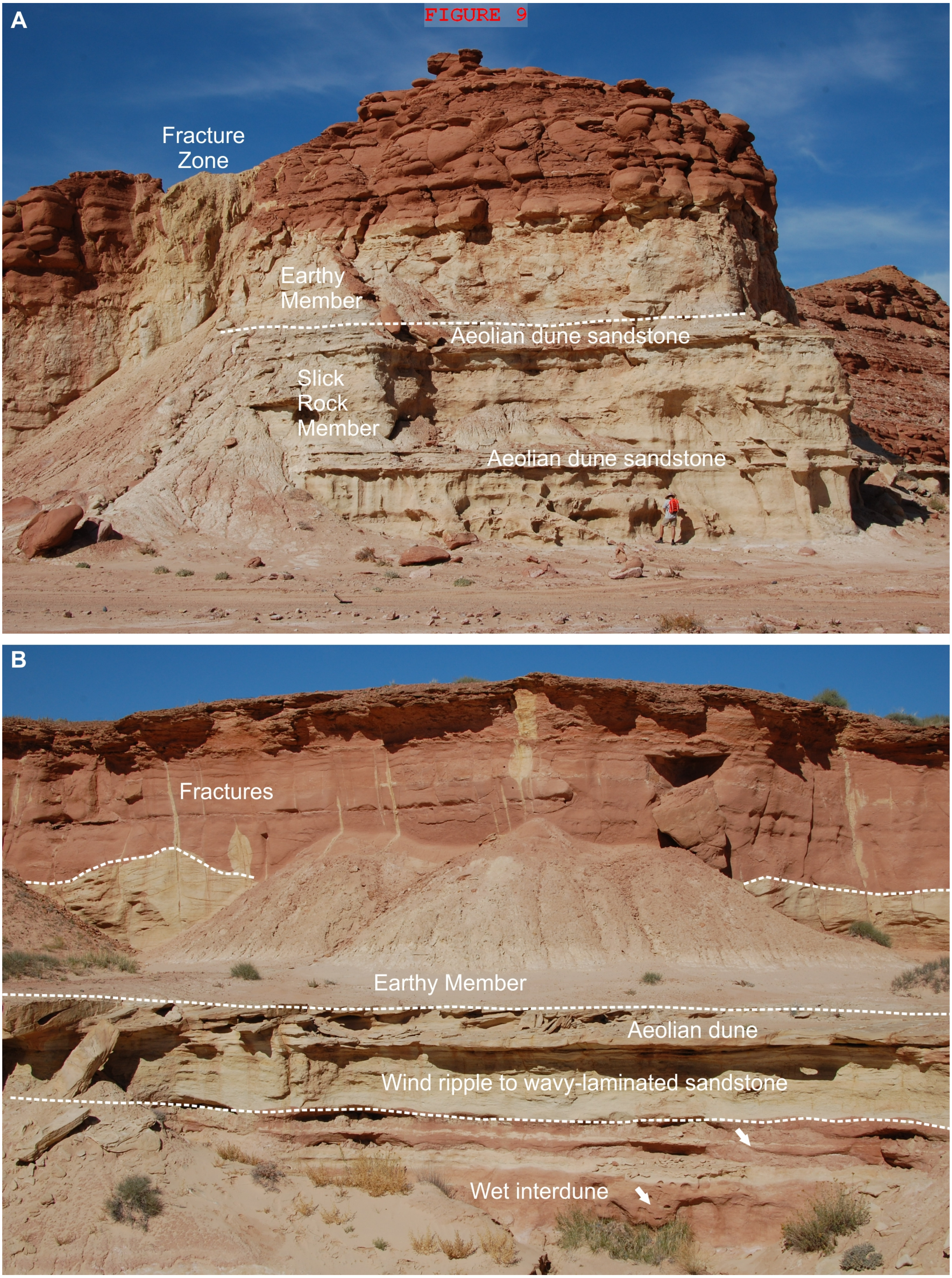
A
Fracture Zone
Earthy Member
Aeolian dune sandstone
Slick Rock Member
Aeolian dune sandstone
B
Fractures
Earthy Member
Aeolian dune
Wind ripple to wavy-laminated sandstone
Wet interdune

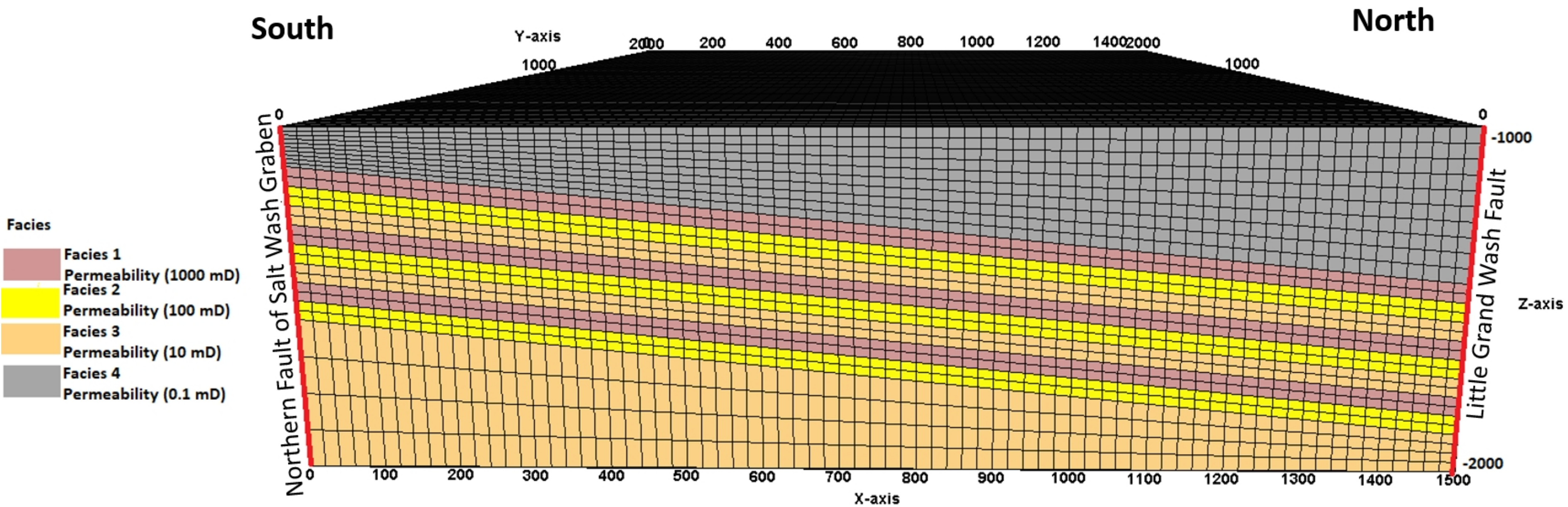
South
North
Y-axis
2000
200
400
600
800
1000
1200
1400
2000
1000
1000
0
0
-1000
-2000
Z-axis
X-axis
0
100
200
300
400
500
600
700
800
900
1000
1100
1200
1300
1400
1500
Northern Fault of Salt Wash Graben
Little Grand Wash Fault
Facies
Facies 1
Permeability (1000 mD)
Facies 2
Permeability (100 mD)
Facies 3
Permeability (10 mD)
Facies 4
Permeability (0.1 mD)

Figure 10

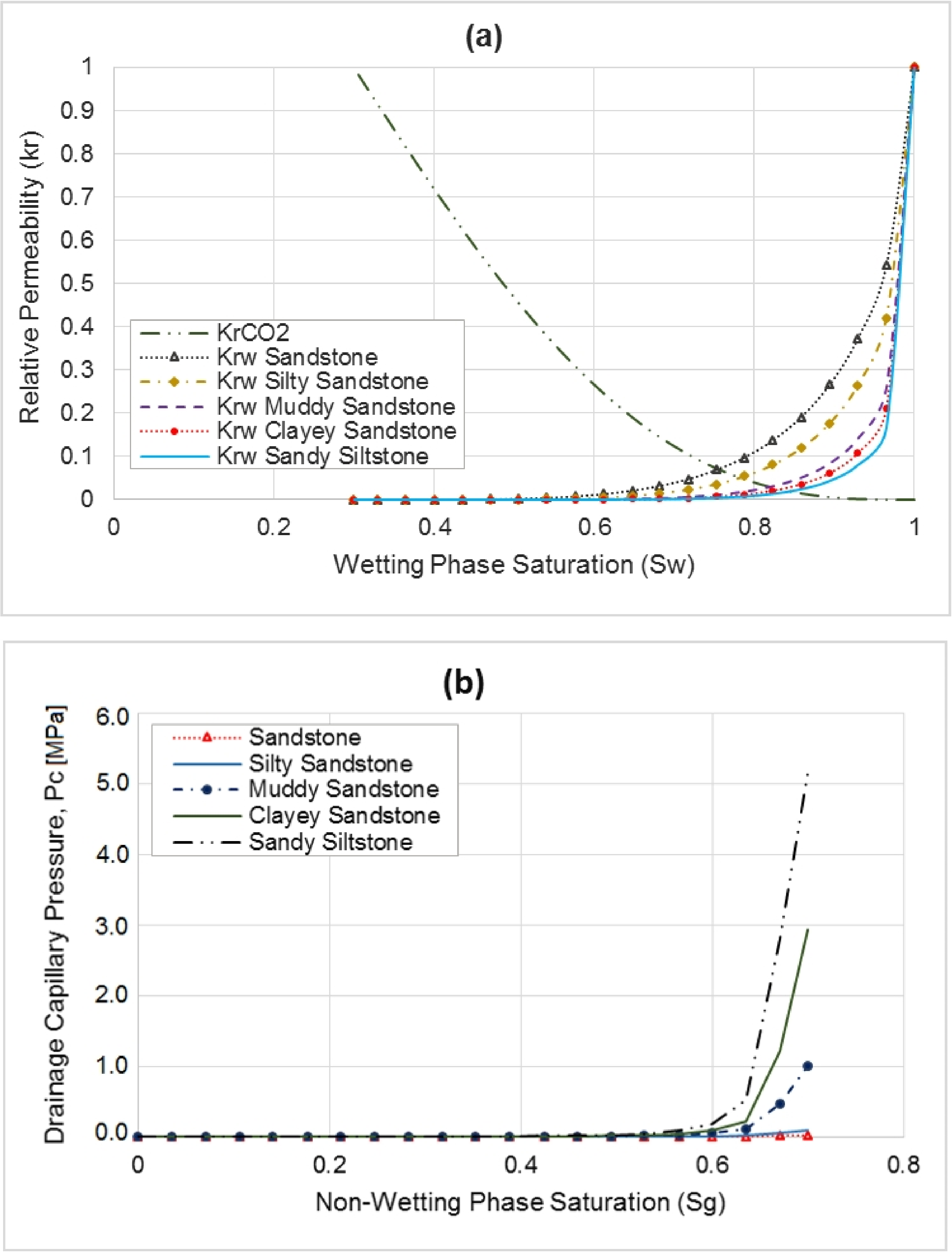
(a)
Relative Permeability (kr)
1
0.9
0.8
0.7
0.6
0.5
0.4
0.3
0.2
0.1
0
0
0.2
0.4
0.6
0.8
1
Wetting Phase Saturation (Sw)
KrCO2
Krw Sandstone
Krw Silty Sandstone
Krw Muddy Sandstone
Krw Clayey Sandstone
Krw Sandy Siltstone
(b)
Drainage Capillary Pressure, Pc [MPa]
6.0
5.0
4.0
3.0
2.0
1.0
0.0
0
0.2
0.4
0.6
0.8
Non-Wetting Phase Saturation (Sg)
Sandstone
Silty Sandstone
Muddy Sandstone
Clayey Sandstone
Sandy Siltstone

Figure 11

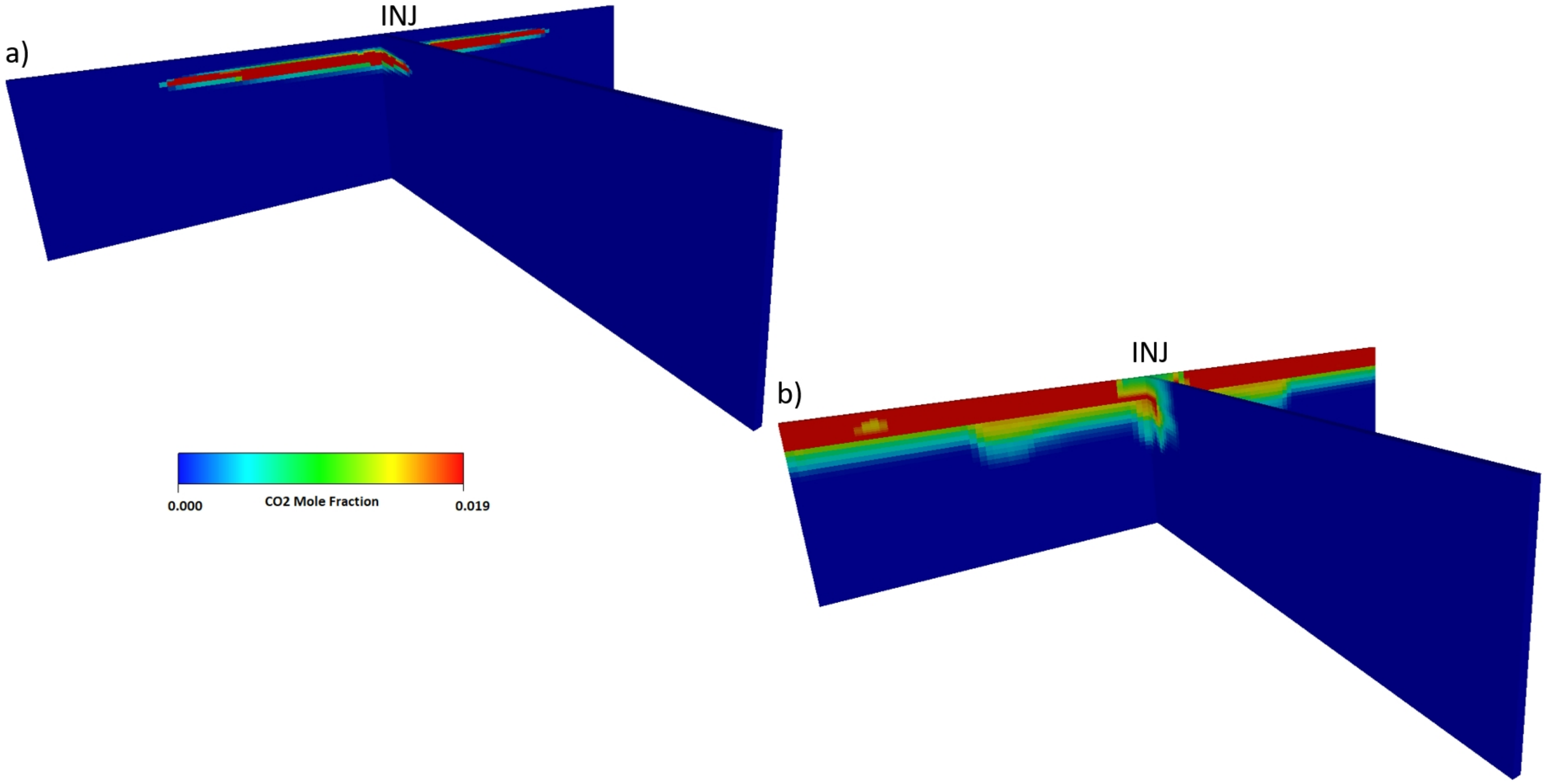

Figure 12

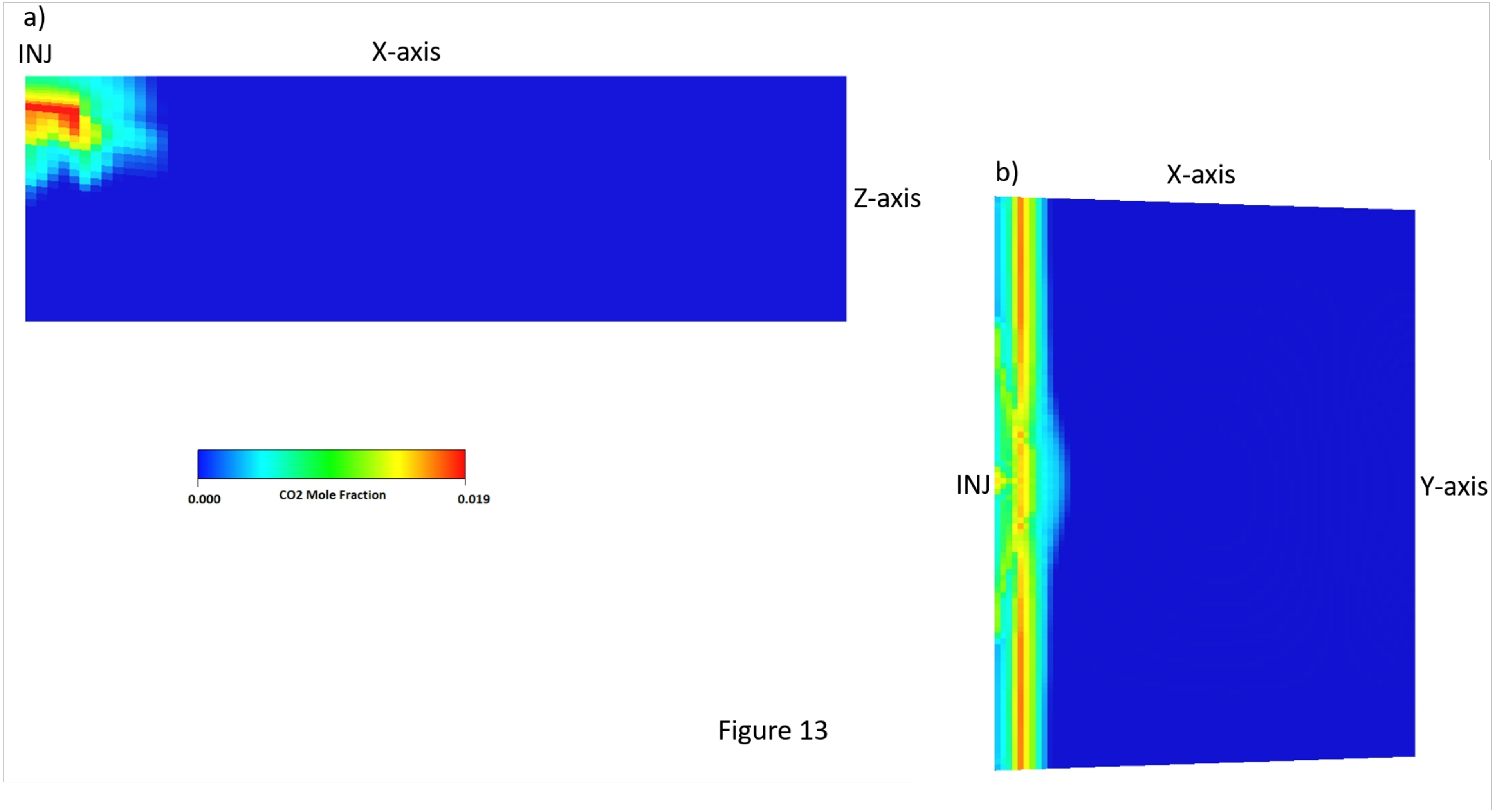
a)
INJ
X-axis
Z-axis
0.000
CO2 Mole Fraction
0.019
b)
X-axis
INJ
Y-axis

Figure 13

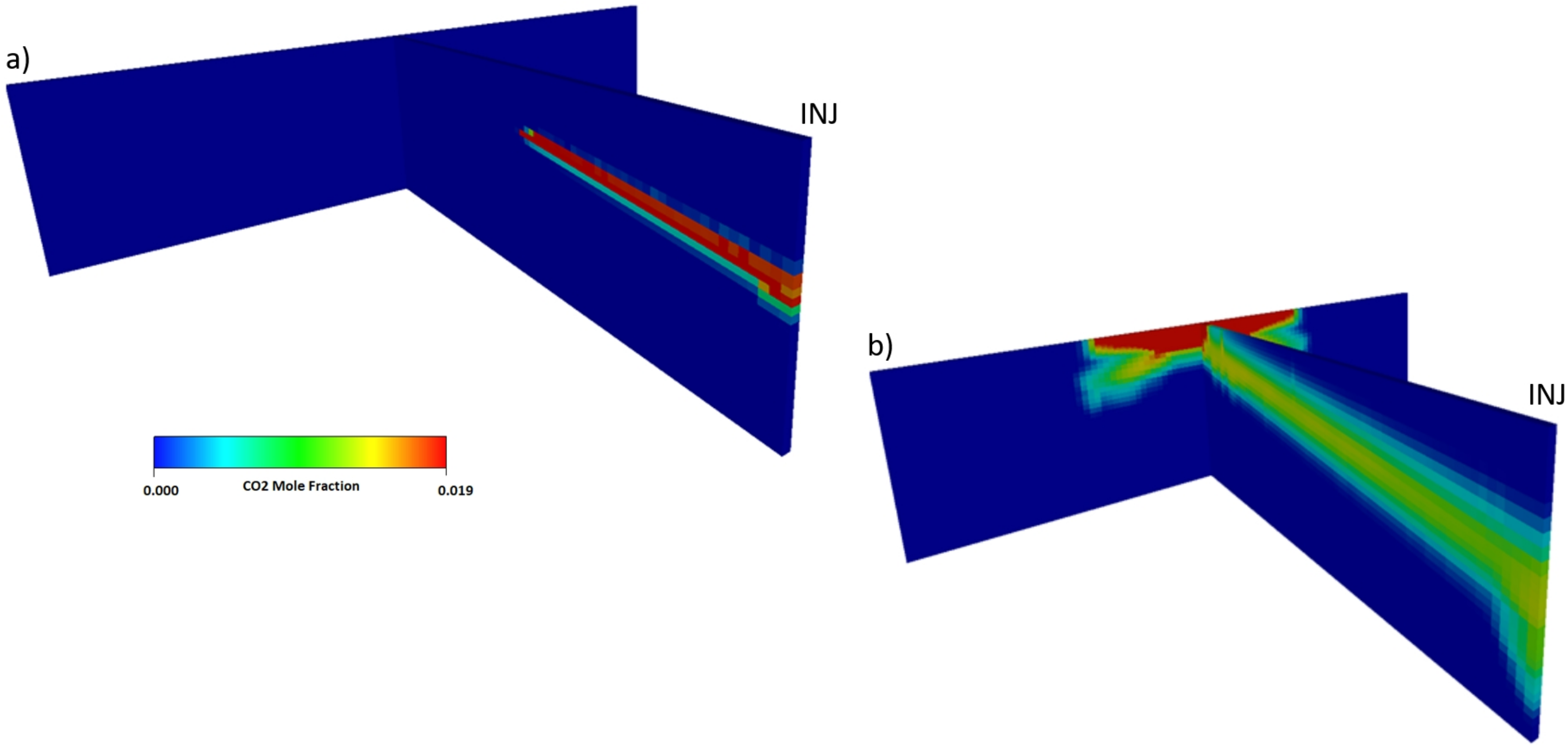

Figure 14

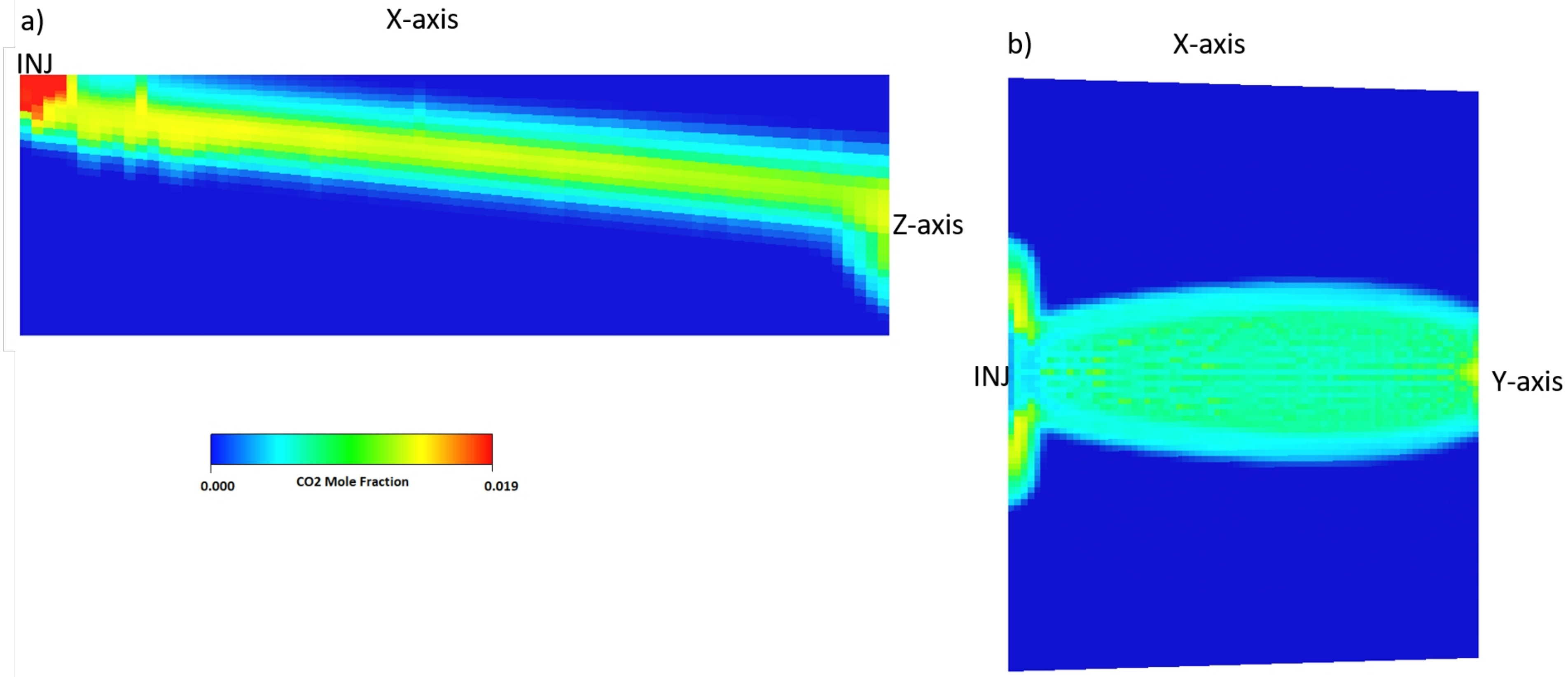
a)
X-axis
INJ
Z-axis
0.000
CO2 Mole Fraction
0.019
b)
X-axis
INJ
Y-axis

Figure 15

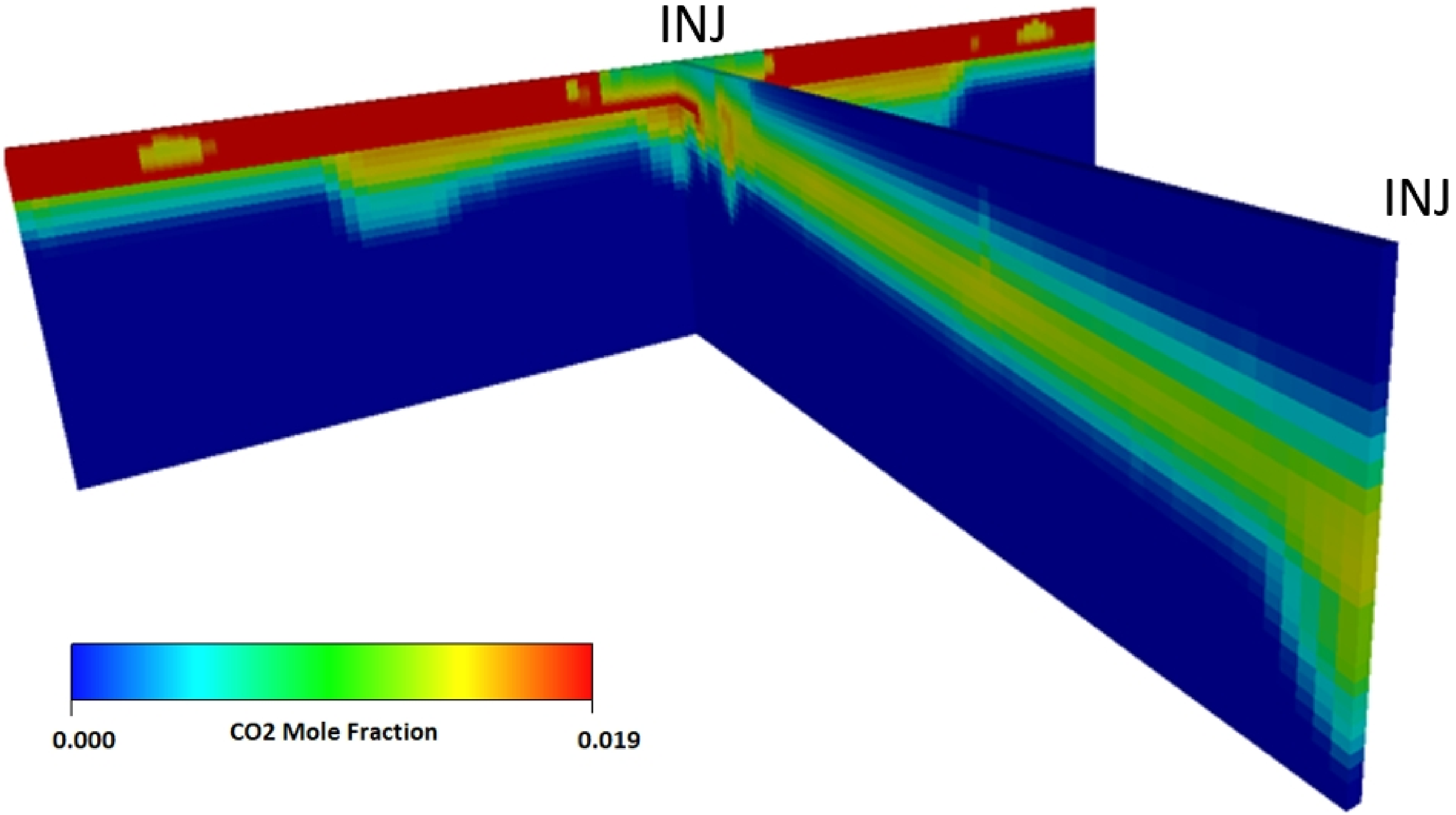

Figure 16

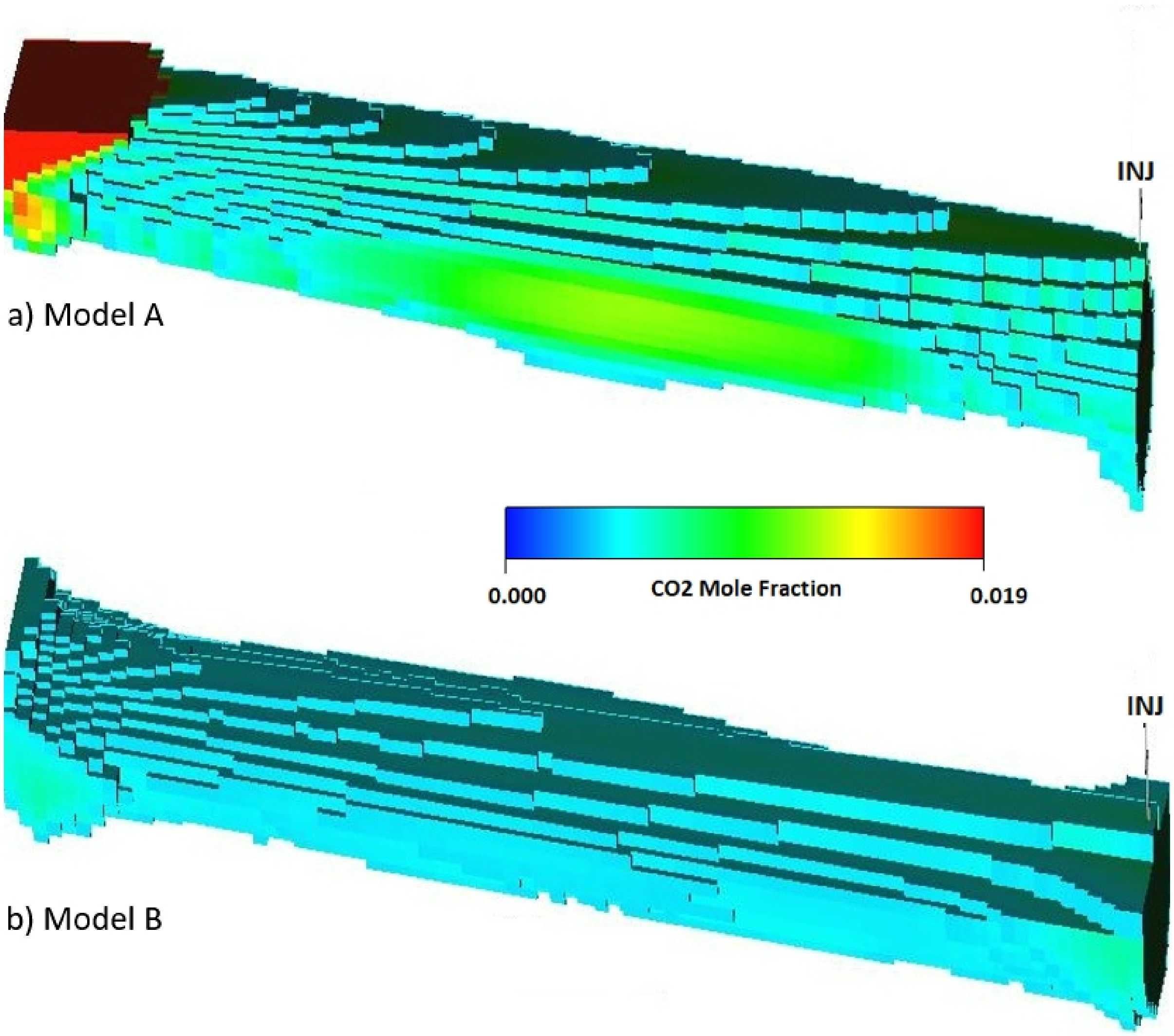

a) Model A

b) Model B

Figure 17

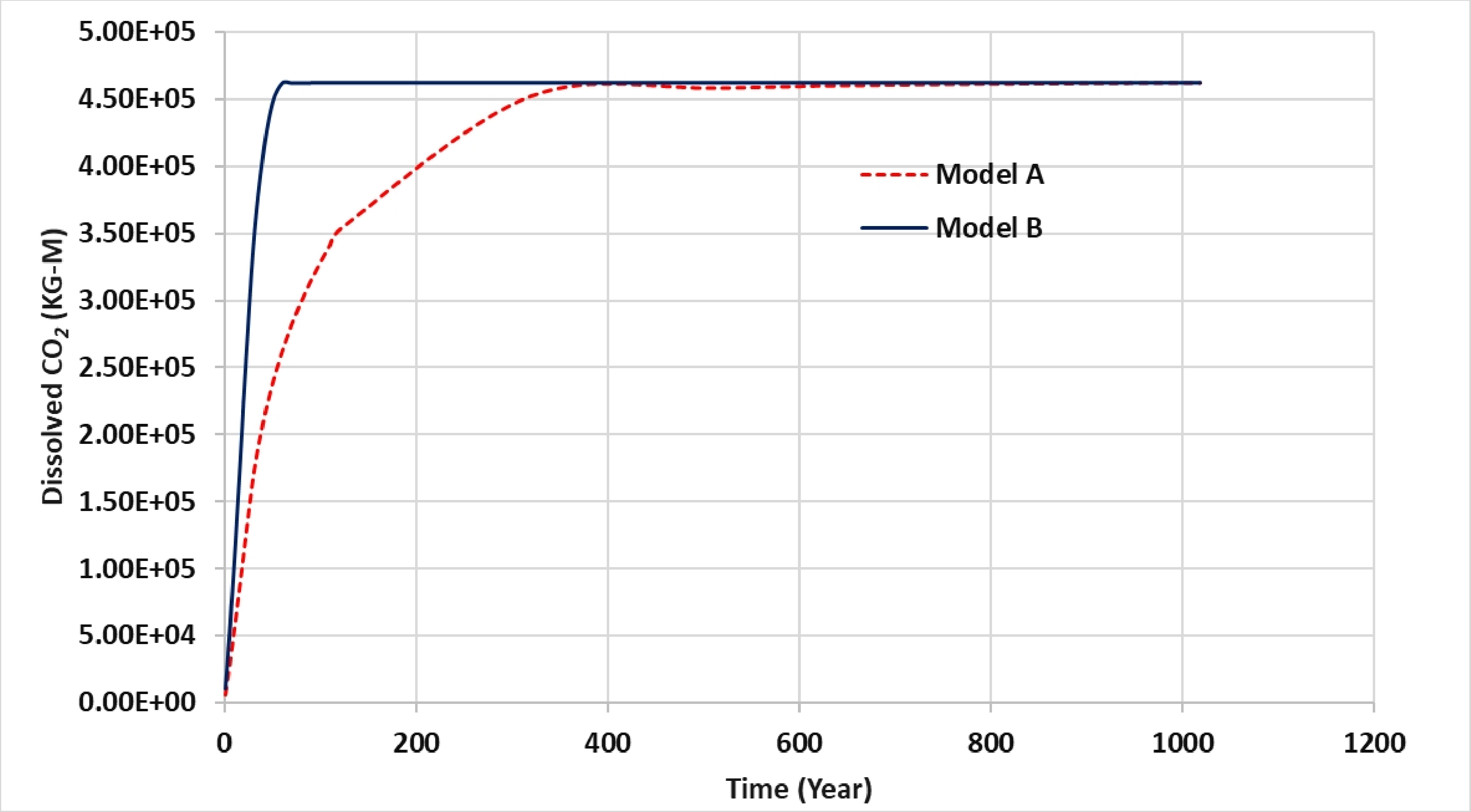

5.00E+05
4.50E+05
4.00E+05
3.50E+05
3.00E+05
2.50E+05
2.00E+05
1.50E+05
1.00E+05
5.00E+04
0.00E+00
Dissolved CO_2 (KG-M)
0
200
400
600
800
1000
1200
Time (Year)
Model A
Model B

Figure 18

Table 1 Lithofacies of the Slick Rock Member

Code	Description	Interpretation	Typical permeability
SHA	Sandstone, high-angle cross-bedded. Tough or tabular cross-bedded with foresets reaching a maximum angle of around 28 degrees. Wedge-shaped or parallel laminated foresets. Composed of fine-medium grained sand, moderately to well-sorted, quartz-rich.	Mobile aeolian dunes with curved or straight crests. Lamination results from grain-flow and grain fall on dune avalanche faces.	1000-10000mD
SLA	Sandstone, low-angle lamination. Typically displays well-developed pin-stripe lamination with alternation of cm-thick, fine-medium sand laminate and mm-thick fine-very fine sand. Quartz-rich, bimodal grain-size distribution.	Migration of wind-ripples on low relief sand sheets or dune aprons	1000-10000mD
SM	Sandstone, massive. Structureless sandstone, or one showing only occasional faint lamination. Very fine to medium grained, sorting generally poor.	Sand accretion in damp interdune areas	100-1000mD
SWL	Sandstone, wavy laminated. Irregular wavy discontinuous lamination, occasionally convolute lamination. Poorly sorted with common silty and very fine-grained sand laminae.	Sand accretion in damp to wet, water saturated, interdune areas	100-1000mD
SMC	Massive or faintly bedded sandstone with ferruginous concretions and wavy lamination, undulating erosion surfaces and channel fills.	Channel fills	100-1000mD
SS	Silty sandstone, discontinuous wavy lamination, massive, occasionally convolute. Very poorly sorted admixture of sand, silt and clay	Deposition on sandflats and sabkha, salt crusts probably important in trapping sediment	0.1-10 mD

	Reservoir (Slick Rock Member)			Topseal (Earthy Member)
Property	lithofacies 1	lithofacies 2	lithofacies 3	lithofacies 4
Porosity [%]	25	15	5	1
Permeability[mD]	1000	100	10	0.1

	Injector location	Location of Perforation	Location of the Faults
Model 1	(i=1, j=50)	(k=11-12)	i:1-1, j:1-100, k:1-30
Model 2	(i=75, j=50)	(k=11-12)	i:75-75, j:1-100, k:1-30
Model 3	(i=1, j=50) and (i=75, j=50)	(k=11-12)	i:1-1, j:1-100, k:1-30 i:75-75, j:1-100, k:1-30

<table>
<tr><th>Model A</th><th colspan="3">Reservoir
(Slick Rock Member)</th><th colspan="3">Topseal
(Earthy Member)</th></tr>
<tr><td>Property</td><td>lithofacies 1</td><td>lithofacies 2</td><td>lithofacies 3</td><td colspan="3">Lithofacies 4</td></tr>
<tr><td>Porosity [%]</td><td>25</td><td>15</td><td>5</td><td colspan="3">1</td></tr>
<tr><td>Permeability[mD]</td><td>1000</td><td>100</td><td>10</td><td colspan="3">0.1</td></tr>
<tr><td>Model B</td><td colspan="5">Reservoir
(Slick Rock Member)</td><td>Topseal
(Earthy Member)</td></tr>
<tr><td>Property</td><td>lithofacies 1</td><td>lithofacies 2</td><td>lithofacies 3</td><td>lithofacies 4</td><td>lithofacies 5</td><td>Lithofacies 6</td></tr>
<tr><td>Porosity [%]</td><td>35</td><td>25</td><td>20</td><td>15</td><td>10</td><td>1</td></tr>
<tr><td>Permeability[mD]</td><td>10000</td><td>1000</td><td>100</td><td>10</td><td>1</td><td>0.1</td></tr>
</table>